5-2012

Thermodynamic Analysis of Polyethylene Glycol Thiol-ene Click Chemistry and Surface Modification of Bacterial Cellulose

Kaan Serpersu
kserpers@utk.edu

To the Graduate Council:

I am submitting herewith a thesis written by Kaan Serpersu entitled "Thermodynamic Analysis of Polyethylene Glycol Thiol-ene Click Chemistry and Surface Modification of Bacterial Cellulose." I have examined the final electronic copy of this thesis for form and content and recommend that it be accepted in partial fulfillment of the requirements for the degree of Master of Science, with a major in Polymer Engineering.

Roberto S. Benson, Major Professor

We have read this thesis and recommend its acceptance:

Kevin M. Kit, Wei He

Accepted for the Council:
Dixie L. Thompson

Vice Provost and Dean of the Graduate School

(Original signatures are on file with official student records.)

Thermodynamic Analysis of Polyethylene Glycol Thiol-ene Click Chemistry and Surface Modification of Bacterial Cellulose

A Thesis Presented for the
Master of Science
Degree
The University of Tennessee, Knoxville

Kaan Serpersu
May 2012

DEDICATION

This work is dedicated to my parents, my two brothers, my sister-in-law, and my niece and nephew. Without their support during these years I would not have made it through. This work is also dedicated to the memory of Zepherus Serpersu, the greatest dog a man could ask for.

ACKNOWLEDGEMENTS

Thanks go to Dr. Engin Serpersu, Dr. Kevin Kit, Dr. Carlos Steren, Dr. Adrianne Norris, Dr. Christopher Stephens, Dr. Wei He, Jonathan Page, Russell Hallman Ryan Hammonds, and William Gazzola.

To my advisor and mentor Dr. Roberto Benson, I cannot understate my thanks for all the guidance, support, and belief in my work and myself.

ABSTRACT

Polyethylene glycol (PEG) has been one of the extensively studied polymers for medical applications. However, the use of PEG can require complicated and low efficiency reactions which can impose limits to potentially useful medical solutions. Click chemistry has recently emerged as a way to avoid these pitfalls by utilizing reactions that are highly efficient and require simple reaction conditions. One such reaction is known as the Michael-addition thiol-ene click reaction (TECC). The combination of PEG with TECC has received some study, but has not been thermodynamically characterized as a click reaction. In this work PEG-TECC reaction kinetics were studied by proton nuclear magnetic resonance (^{1}H-NMR) and quartz crystal microbalance with dissipation (QCM-D) in order to assess the components ability to form complex final products quickly and with minimal side products. From these kinetic studies, the energy of activation for PEG-TECC was determined. The reaction was concluded to follow the click chemistry philosophy and is viable for future applications. The energy of activation was determined to be 75 kJ/mol. Bacterial cellulose (BC) is a naturally produced polymer and has been shown to have great potential for bone, cartilage, and vascular tissue engineering applications. In order to incorporate PEG-TECC, BC was modified on the surface with acrylate functionalities to provide a Michael-addition TECC starting point. The surface of BC was modified with TECC components in a simple, straightforward manner, keeping in line with the philosophy of click chemistry. This modification allows BC to incorporate PEG to form a BC with PEG co-hydrogel and can be easily modified due to the variety allowed by incorporation of both TECC and PEG. This system allows for the combination of the strength of BC, the versatility of PEG, and speed and efficiency of TECC into one product without the need for complex reaction conditions. The surface modification of BC was confirmed with a colorimetric assay, Fourier transform infrared spectroscopy-attenuated total internal reflectance (FTIR-ATR), and titration.

TABLE OF CONTENTS

LIST OF TABLES

Table Page

LIST OF FIGURES

LIST OF ACRONYMS

Acronym	Full Word
^{1}H-NMR	Proton Nuclear Magnetic Resonance
^{13}C-NMR	Carbon-13 Nuclear Magnetic Resonance
AIBN	2,2'-Azoisobutyronitrile
ATCC	American Type Culture Collection
BC	Bacterial Cellulose
CEA	2-Chloroethyl Acrylate
Cu(I)	Copper Halide
D_2O	Deuterium Oxide
DDT	1,10-Decane-Dithiol
DI	Deionized
DMPA	Dimethoxy-2-Phenyl Acetophenone
DSS	4,4-Dimethyl-4-Silapentane-1-Sulfonic Acid
E_a	Energy of Activation
FDA	Food and Drug Administration
FTIR	Fourier Transform Infrared Spectroscopy
FTIR-ATR	Fourier Transform Infrared Spectroscopy Attenuated Total Reflectance
HCl	Hydrochloric Acid
HDPE	High Density Polyethylene
LDPE	Low Density Polyethylene
LLDPE	Linear Low Density Polyethylene
MW	Molecular Weight
NaOH	Sodium Hydroxide
NMR	Nuclear Magnetic Resonance
PE	Polyethylene
PEG	Polyethylene Glycol
PEG-2ACY	Polyethylene Glycol Diacrylate
PEG-ACY	Polyethylene Glycol Acrylate
PEG-SH	Polyethylene Glycol Thiol
PEG-TECC	Polyethylene Glycol Thiol-ene Click Chemistry
PEO	Polyethylene Oxide
PPO	Poly(2,6-Dimethyl-1,4-Phenylene Oxide)
QCM-D	Quartz Crystal Microbalance with Dissipation
SAM	Self-Assembled Monolayer
TECC	Thiol-ene Click Chemistry
TIR	Total Internal Reflectance
UDP-G	Uridine Diphosphate Glucose

CHAPTER 1
INTRODUCTION

Polymers are a core material group that has seen innumerable applications from structural supports, medical implants, a wide range of consumer products, and composites with other materials. Established medical applications for polymers include serving as tissue engineering scaffolds and drug delivery systems. Polymers can be formed into hydrogels, degradable scaffolds, non-degradable scaffolds, fibers formed by melt blowing or electro-spinning, copolymers, and other products in order to tackle these applications. Polymers can be considered either synthetic, made in the lab, or natural, found in nature, materials. Polyethylene glycol (PEG) is one of the most heavily utilized synthetic polymers for medical applications and is approved by the Food and Drug Administration (FDA) for internal use. Bacterial cellulose (BC) is a naturally produced polymer and is quickly emerging as a successful scaffold for bone, cartilage, and vascular tissue engineering. The combination of PEG with BC would provide a scaffold with the mechanical strength and stability of BC with the extensively tailored properties of PEG. However, linking the two together requires the surface modification of BC which would provide easy and efficient PEGylation. Click chemistry and its philosophy provide this link.

Click chemistry theorizes that the synthesis of complex products can be done by using key reactive functional groups that are fast, efficient, and easy to purify. It is a recent philosophy, cropping up in 2001 by an article by K.B. Sharpless et al. and has since gone on to permeate throughout the scientific community, both academic and corporate. The principles outlined by click chemistry avoid needlessly complicated reactions that are slow, low efficiency, and require chromatography purification. Thiol-ene click chemistry (TECC) is one branch of click chemistry which revolves around reacting thiols and alkenes with either a free radical or base/nucleophilic catalyst. PEG can be modified with TECC components at its terminal ends, thus taking the benefits allowed by TECC and PEG. This requires PEG molecules with thiol end groups (PEG-SH) and PEG with alkenes which can be electron rich or electron poor, such a PEG with acrylate end groups (PEG-ACY). The work presented here is the thermodynamic analysis of PEG Michael-addition thiol-ene click chemistry (PEG-TECC), including reaction kinetics to determine the reaction rate constant (k) and the energy of activation (E_a). BC was then surface modified to allow for PEG-TECC functionalization. This thesis presents the thermodynamic characterization of PEG-TECC and the surface modification of BC to easily combine PEG-TECC and BC to create a tissue engineering scaffold that has the benefits of BC, PEG, and TECC.

Included in this body of work is the theory and background of polymers, PEG, click chemistry, TECC, BC, and the analytical techniques used during the course

of this work (Chapter 2). Analytical techniques include proton nuclear magnetic resonance (^{1}H-NMR), quartz crystal microbalance with dissipation (QCM-D), colorimetric assays, Fourier transform infrared spectroscopy-attenuated total reflectance (FTIR-ATR), and titration. All experimental methods and materials are laid out as plainly as possible for future work (Chapter 3). The results for PEG-TECC characterization and BC surface modification are showcased in Chapter 4 with a detailed discussion of the data in Chapter 5. Finally, conclusions drawn from this work and suggested future work is discussed in Chapter 6.

CHAPTER 2
THEORY AND BACKGROUND

2.1 Polyethylene Glycol (PEG)

2.1.1 Introduction to Polymers

In the simplest terms, polymers are materials which are made up by a definable repeat unit called a monomer [1]. The key to this definition is *definable repeat unit*. A simple example to expand on this idea is polyethylene (PE) (Figure 1). PE comes in multiple commercial forms, including high density PE (HDPE), low density PE (LDPE), and linear low density PE (LLDPE). The structural difference between the three examples given is the extent of chain branching and length of the branched chains [2]. This seemingly insignificant difference in structure has dramatic effects on material properties, percent crystallinity, moisture permeation, and potential applications. However, the commonality between all three is the repeat unit, ethylene (IUPAC name: ethene) (Figure 2). The different permutations of PE described are synthesized from the base monomer ethylene, and the type of PE created depends on the processing conditions utilized, with a general polymerization scheme following vinyl addition polymerization. This philosophy can be visualized by the polymer triangle, linking material properties, processing, and structure (Figure 3). Material properties of polymers can be controlled by modifying the structure which can be controlled by the processing conditions used for synthesis. Hence, HDPE, LDPE, and LLDPE all come from the polymerization of ethylene, but end up with different materials properties due to changes in processing affecting the chemical structure of the final product. By controlling processing and modifying structure, polymers with desired material properties can be synthesized for select application.

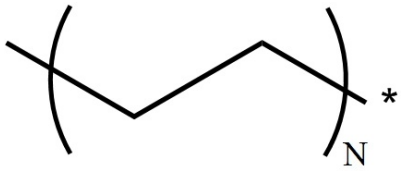

Figure 1: Polyethylene, with N > 10

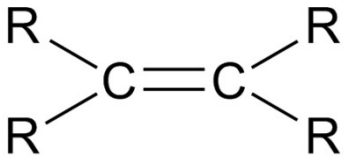

Figure 2: Ethylene, starting monomer for PE, with R = H

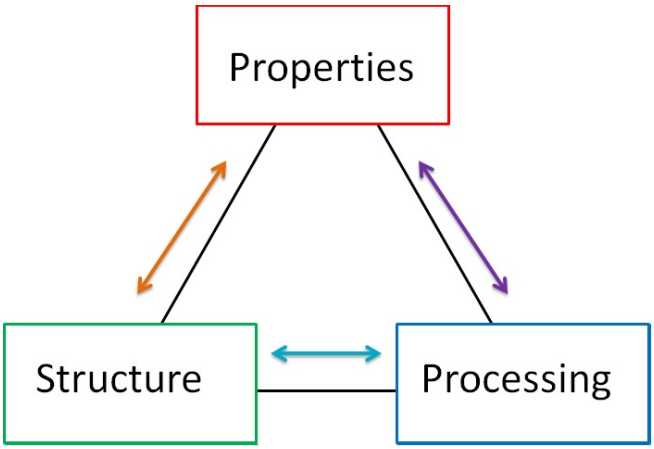

Figure 3: Polymer triangle

2.1.2 PEG Fundamentals

PEG (Figure 4) is one of the most commonly used polymers that is commercially available. Through a wide variety of physical and chemical modifications, the available applications for PEG are numerous. Applications range from work in the medical field such as drug delivery vehicles and non-fouling coatings for implants, to other everyday items such as toothpaste and food additives [3]. Reasons for the use of PEG depend on the application, but a short summary is necessary for the discussions presented in this thesis. As discussed for PE, PEG is polymerized from a definable repeat unit. The monomer for PEG is ethylene glycol (Figure 5) (IUPAC name: ethane-1, 2-diol).

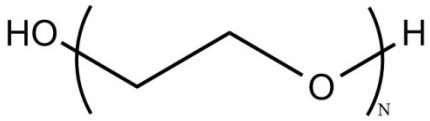

Figure 4: Polyethylene glycol, with N > 10.

Figure 5: Ethylene glycol, monomer used to produce PEG.

PEG is available in many forms, depending on molecular weight (MW) and end functional group. If the MW is below 20,000 g/mol, then it is given a commercial name of PEG. However, if the MW is raised above 20,000 g/mol then it is typically referred to as polyethylene oxide (PEO) [4]. PEG and PEO are chemically identical, but due to differences in chain length and branching, they are used for different applications [4].

PEG has been functionalized with a wide variety of functional groups, replacing the hydroxyl groups normally found at the terminal ends of PEG. Functional groups have included thiols, acrylates, amides, amines, carboxylic groups, and even ringed structures such as epoxide or maleimide. These modifications have been implemented to make monofunctional, homobifunctional, heterobifunctional, 4-arm, and 8-arm variants of PEG, all of which are commercially available through multiple vendors. For this work, PEG-SH (Figure 6) and PEG-ACY (Figure 7) were used for characterization of PEG-TECC. The reaction of PEG-SH and PEG-ACY is shown in Figure 8.

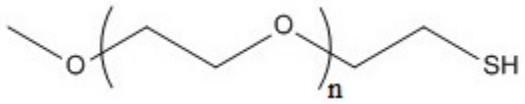

Figure 6: Polyethylene glycol thiol (PEG-SH), n > 10

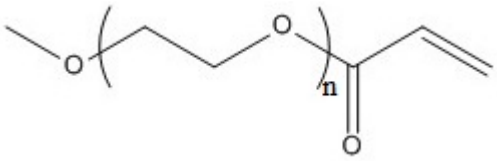

Figure 7: Polyethylene glycol acrylate (PEG-ACY), n > 10

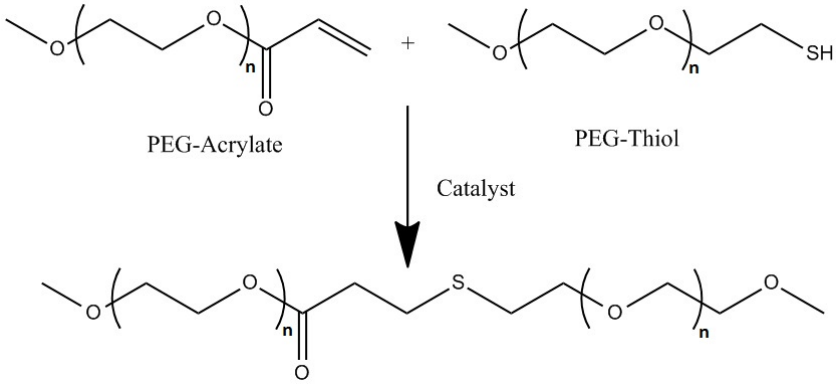

Figure 8: PEG-TECC reaction studied in this work

2.1.3 Properties and Applications

PEG, in its normal configuration, is a hydrophilic polymer which forms an ether linkage between monomers during synthesis. PEG is soluble in water, forms complexes with metal cations, highly mobile, nontoxic, FDA approved for internal consumption, can easily form into a hydrogel, mechanical properties which can be tailored to match tissue engineering parameters, capable of acting a drug delivery or cell encapsulation device, and hospitable to biological materials [3-10]. Because of the vast number of options for PEG hydrogels and copolymers, a short summary of mechanical properties would unfairly pigeon-hole PEG and

exclude the significant number of applications available to PEG. As an example, in a 2005 article by Mann et al., PEG hydrogels were made with varying concentrations of crosslinking agent. This studied showed that neurite extension of PC-12 cells were heavily dependent on the mechanical properties of the PEG hydrogel, with hydrogels with elastic modulus of 20 kPa showing significantly greater neurite extension than hydrogels with an elastic modulus of 400 kPa [11]. PEG hydrogels with collagen have been shown to have stiffness values as low as 0.4 kPa [12].

As mentioned previously, there has been significant research in PEG hydrogels for medical applications. A hydrogel is a 3D network of cross-linked polymer chains that swells in the presence of water. These cross-links can be made up of covalent bonds, chain entanglements, hydrogen or van der Waals bonds, or crystallites [3, 5]. Due to PEG's inherent biocompatibility and number of configurations, PEG has become an attractive polymer for hydrogel creation. Some of the many other applications of PEG include the following examples. PEG has been used for surface modification of polysaccharides and immobilization of proteins [4, 13]. PEG hydrogels using TECC components have been studied for drug delivery vehicles, with great success [8, 14]. PEG can also be joined into a copolymer for either drug delivery dendritic block copolymers [15] or a 'smart' hydrogel system [16]. In 'smart' hydrogels, the gelation of the hydrogel occurs only in response to a select stimulus, such as temperature or pH [3, 5, 17]. A medically related example of a 'smart' hydrogel is a PEG copolymer hydrogel which gels at physiologic temperature [16]. The choice of PEG for the surface modification for BC opens up enormous potential for future applications due to the 'jack-of-all-trades' nature of PEG.

2.2 Click Chemistry

2.2.1 Click Chemistry Philosophy

Click chemistry is a recently explored area of chemistry that was defined by a seminal article by K.B. Sharpless et al. in 2001 [18]. Since this article, there has been widespread research into unlocking the potential of click reactions and defining the reactions that meet the criteria. The philosophy of click chemistry is one of both simplicity and function over form. Click chemistry can be thought of, not as a reaction, but as a combination of a set of rules followed by certain reactions and the mindset of the researcher. These rules serve as guidelines to help better illustrate the power of click components and the subsequent applications that are opened up. Click chemistry seeks functional groups which will react together in the fastest and most straightforward way possible while following the rules of click chemistry. A list of the proposed click chemistry rules can be found below in Table 1 [18].

Table 1: Reaction requirements for Click Chemistry.

Reaction is quick and efficient
Water or no solvent
Side products removed without chromatography
Insensitive to water and oxygen
Modular and wide scope
Regiospecific and Stereospecific
Products stable under physiological conditions

Pursuing click chemistry as a way of creating products requires a mindset that values function over complex and patentable reactions [19]. In both his 2001 article and a follow-up article in 2003 which discussed the impact of click chemistry on the pharmaceutical industry, Dr. Sharpless discussed the need for simpler chemical synthesis in creating new drugs [18, 19]. Click chemistry and its principles came from studying the best teacher available to scientists; nature. The primary target of synthetic chemists is to synthesize analogs of secondary metabolites to act as drugs for various diseases or infections [18]. However, this has required multiple intense synthesis steps, with years of research and immense funding put into the creation of one of these analogs. An example given by Dr. Sharpless is that of Meropenem®, a derivative of the antibiotic Thienamycin, which took over 6 years of research to synthesize after the successful synthesis of Thienamycin [18]. By taking click chemistry and applying its principles, both drugs and complex polymers can be made with a few simple steps. As will be shown in this thesis with the modification of bacterial cellulose, even surface modifications of polymers can be performed using this simple philosophy. The axiom of click chemistry has already permeated into many corners of the academic and corporate research world, with applications ranging from biomedical technology [20], hydrogels [16, 21], drugs [22, 23], fluorescent labeling [24], photovoltaics [25], and the conversion of vegetable oil biopolymers [26].

Several reactions have been accepted as being “click” reactions; the most extensively studied being the copper-halide (Cu(I)) catalyzed Huisgen 1,3-dipolar cycloaddition reaction between an azide and alkyne (Figure 9).

Figure 9: Generalized Cu(I) click reaction between azide and alkyne, with variable R and R’ groups.

One intriguing characteristic that makes click chemistry so unique is the ability to tailor the components to fit specific applications. The versatility of these click

reactions stem from the variety of R and R' groups attached to the reacting functional groups. Groups attached to either the azide or alkyne in the Cu(I) catalyzed reaction have included diverse compounds such as benzene rings, steroids, carboxylic acids, phenol rings, cellulose, esters, thiols, and many others [18, 20-25, 27-31].

The Cu(I) reaction, while versatile and important for studying click chemistry, was not the subject of this research for one reason; the explosive nature of azides. This safety issue could impose limitations on future biomedical applications. This concern was easily overcome by examining the potential for a lesser known click reaction, thiol-ene coupling. This reaction has two configurations, which depend on the groups attached to the thiol and alkene functional groups and their effect on steric hindrance and electron availability of the thiol or alkene. The two mechanisms which will be discussed are the free radical and Michael-addition types, described in detail in sections 2.2.2.1 and 2.2.2.2, respectively.

2.2.2 Thiol-ene Click Chemistry (TECC)

TECC refers to click reactions that take place between a thiol and alkene, either by free radical or base/nucleophilic catalyzed mechanisms (Figure 10). TECC encompasses the free-radical and base/nucleophilic catalyzed versions as both have been shown to fit the click chemistry criteria. TECC has been the subject of multiple review articles which highlight this ability [32-36]. Similar to the Cu(I) catalyzed reaction, a variety of thiol-ene components have been shown to follow the rules summarized in Table 1. The catalyst required, and thus type of mechanism the reaction will follow, is dependent on the thiol and alkene reagents. Reactions between electron rich alkenes and thiols would be best suited for free-radical initiated reactions. Electron poor alkenes, such as those found in acrylates, are optimal for the base/nucleophilic catalyzed reaction, following a Michael-addition mechanism. These two distinct forms of TECC will now be explained in detail in hopes of elucidating this exciting area of research.

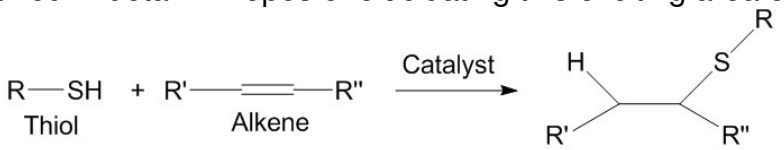

Figure 10: General TECC reaction

2.2.2.1 Free Radical Type Thiol-ene Click Reaction

The free radical form of TECC has been successfully developed into a well-defined reaction, able to form large and complex products quickly and efficiently. Several articles have been published that help to define the effects of different configurations on the properties of this reaction including production of large scale dendrimers [37], effects of initiators and chemical structure on conversion and kinetic rates [38], controlling activation energy by incorporation of gold

particles [39], and the thermal and photoinitiated polymerization and mechanical properties of formed copolymers [40, 41].

The agreed upon mechanism for this reaction involves the creation of a free radical as its first step. This requires the use of a photo- or thermal initiator. This necessitates reactive sites which are electron rich, under heavy ring strain, and are not sterically hindered [33]. Compounds such as norbornene [33], vinyl ethers [33], allyl halogens [38], or electron rich alkynes [42] have been shown to undergo the free radical TECC reaction quickly and to near completion, depending on the initiator. Reactions using photoinitiators such as 2,2-dimethoxy-2-phenyl acetophenone (DMPA) have shown conversions ranging from 95-100%, while reactions using a thermal initiator, 2,2'-azoisobutyronitrile (AIBN), showed lower, but still near complete conversions between 86 – 89% [38]. Because the generation of a free radical *in-vivo* may prove difficult, future applications for this project involving biomedical implants and the use of bacterial cellulose could be limited. For this reason, the Michael-addition type was selected as the reaction of study. However, the work done here can easily be switched to PEG components which proceed by free radical initiation, if desired. Components for that project would be PEG-SH and PEG-alkyne, both of which are commercially available from many suppliers.

2.2.2.2 Michael-Addition Type Thiol-ene Click Reaction

The Michael-type addition reaction has been well documented, with multiple recent articles discussing the effects of solvent, reagents, catalysts, abilities for surface modifications, and reagents on reaction yields and time as will now be described [43-48].

Reactions taking place between electron deficient carbon-carbon double bonds and thiols are best suited for base/nucleophilic catalyzed reactions dubbed Michael-addition TECC. The electron deficiency of the carbon-carbon double bond found in acrylates comes from the electronegativity of the neighboring ester linkage, creating partially positive charges on the alkene bond. PEG-ACY molecules reacting with PEG-SH are best handled by creation of a highly reactive, deprotonated thiol by a basic or nucleophilic catalyst (step 2 of Figure 11 and step 1 of Figure 12). The creation of this deprotonated thiol has been the subject of some debate when spoken in context of a nucleophilic catalyst. The proposed mechanism for thiolate creation originally involved phosphine catalysts but was also proposed for some primary and secondary amines [48]. The thiolate created in Figure 11 would then proceed by the agreed mechanism shown in Figure 12. This mechanism involves the creation of a side product (step 2 of Figure 11) along with the thiolate to propagate the reaction. However, a recent study showed that this side product was only measureable by mass spectroscopy if there was a substantial excess of amines over thiols, due to thiolates being better nucleophiles than amines [47]. This deprotonated thiol goes

on to react with the electron deficient alkene in an anti-Markovnikov fashion, setting up a secondary carboanion (step 2 of Figure 12). The catalyst then returns for the finale, protonating the carboanion into a stable final product and regenerating the catalyst (step 3 of Figure 12) [33,38,47,48].

The need for electron-deficient alkenes comes from the creation of the thiolate (Figure 11) and reaction between the thiolate and the alkene (second step in Figure 12). This electron deficiency of the alkene allows for the high affinity between the electron donating thiolate and alkene. Once this new bond forms, an enolate is left until proton abstraction from the now acidic catalyst [47, 48]. For the reaction shown, ethylenediamine acts a nucleophilic catalyst, as is common for primary amines in TECC reactions [48]. The effect of different nucleophilic and basic catalysts has been studied by Hoyle et al., comparing the catalytic power of primary, secondary, and tertiary amines and phosphines. For both amines and phosphines, increasing the nucleophilicity of the catalyst increased the rate of the reaction, allowing for completion extremely quickly, while tertiary amines were unable to start the reaction due to limited nucleophilicity and increased steric hindrance to the nitrogen [48].

The structure of the alkene and thiol also affects the reaction kinetics, similar to the free radical TECC reactions discussed in section 2.2.2.1. Thiols with lower pK_a values and thus more acidic, exhibited faster kinetics than more basic thiols due to ease of deprotonation. The structure of the alkene also played a significant role in reaction rates, showcased by propyl maleimide, which contains two electron withdrawing carbonyls and a ring strained alkene, completing the reaction in only a few seconds. This is in stark contrast to methacrylate alkenes, which did not significantly react due to steric hindrance and inductive stabilization by the methyl side group attached to the alkene [48].

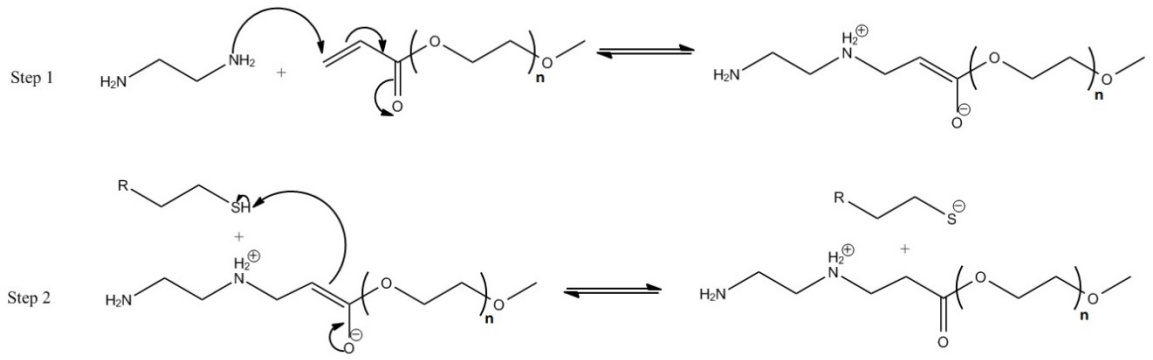

Figure 11: Speculated mechanism for creation of thiolate with nucleophilic catalysts.

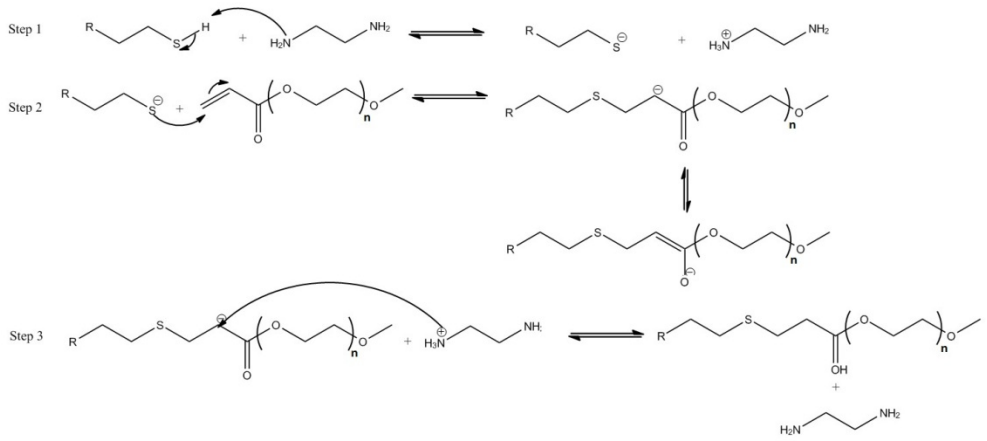

Figure 12: Mechanism for PEG-TECC reaction with base catalyst.

2.2.3 Thermodynamics

Thermodynamics is the branch of science which, at once, can be used to describe chemical behavior and polymer collapse in poor solvents. Thermodynamics is the driving force behind the power of TECC. One of the key rules followed by click chemistry reactions is the ability for them to finish quickly and with high efficiency [18]. This implies thermodynamically driven reactions that have low energies of activation and high affinity between reactant groups. Thermodynamics, while a nightmare for some students, can be summarized with the classic equation relating free energy (ΔG) with enthalpy (ΔH), entropy (ΔS), and temperature (T) (Equation 1). The free energy available in a system defines whether a reaction will be spontaneous or not. In simpler terms, the reaction will not proceed without the availability of free energy. This is given by Equation 1 only when there is a negative value for ΔG, meaning there is free energy available in the system [49, 50].

Equation 1: Classic thermodynamic equation for free energy

$$\Delta G = \Delta H - T\Delta S$$

Reaction rates are known to be dependent on temperature, pressure, reagent concentration, and the presence of a catalyst. Concentration's effect on reaction rates can be summarized as the effect of probability. By changing the concentration of reagents, the probability that the molecules will collide for reaction also changes. Thus, increasing concentration will see faster reaction rates, while decreasing concentration will slow the reaction due to likewise changes in probability for collision [49]. The effect of temperature can be seen mathematically by studying Equation 1. Increasing temperature will enhance the effect of the second term, which is negative assuming positive entropy, in driving the free energy into a spontaneous state. However, this is not the only effect of temperature, as increasing temperature will also increase the chaotic motion of

the molecules. This increase in chaotic motion gives an increase to the entropy of the system [51]. However, as the reaction proceeds, the number of molecules available to react diminishes, lowering the entropy of the system. The presence of a catalyst, a molecule which is not used up in the reaction and remains once the reaction is complete, serves to lower the energy of activation to increase the reaction rate [52].

Free energy and chemical equilibrium are intimately related. The chemical equilibrium constant (*K*) of a reaction is the relationship between concentrations of products to reactants and illustrates the extent of a reaction (Equation 2). Reactions which are favorable, or made favorable by the addition of a catalyst, will have chemical equilibriums greater than one while unfavorable reactions will be less than one [53].

Equation 2: Chemical equilibrium constant (K)

$$K = \frac{[Products]}{[Reactants]}$$

This equilibrium constant, *K*, and the standard free energy (ΔG^0) of reactions can then be related by Equation 3. Study of Equation 3 highlights the connection between free energy and chemical equilibrium, with *K* being larger than one for reactions with negative free energy and *K* less than one for reactions with positive free energy. Combination of Equation 1 and Equation 3, at the standard state, could then be combined to derive the van't Hoff equation (Equation 4).

Equation 3: Relationship between the standard free energy and chemical equilibrium constant.

$$\Delta G^0 = -RTln(K)$$

Jacobus van't Hoff developed the mathematical model to show how the chemical equilibrium constant was dependent on the temperature of the reaction, dubbed the van't Hoff equation (Equation 4). Work by van't Hoff made it possible to determine the standard enthalpy (ΔH^θ) and standard entropy (ΔS^θ) of a reaction by simply plotting the natural log of K (ln(*K*)) against 1/T [49, 50]. Later work by van't Hoff's good friend Svante Arrhenius, gave a proposed explanation for the dependence of reaction rates with temperature. Based on the differential form of the van't Hoff equation (Equation 5), Arrhenius proposed that the chemical rate coefficients, both forward and reverse, were based on the energies of the "activated" states (Equation 6). This energy was called the energy of activation, and was the "hump" which was needed to be overcome before a reaction could go to the next step [49]. The rate determining step of a reaction is the slowest step, or transition, in the reaction owing to a large energy of activation [51, 52]. His work, which related the kinetic rates, temperature, and energy of activation,

gave his namesake equation, the Arrhenius equation (Equation 7) [49, 50]. The Arrhenius equation gives a relationship between the reaction rate constant (*k*) to an Arrhenius pre-exponential function (*A*), E_a, the gas constant (*R*), and temperature (T).

Equation 4: Derived van't Hoff equation

$$\ln(K) = -\frac{\Delta H^{\emptyset}}{RT} + \frac{\Delta S^{\emptyset}}{R}$$

Equation 5: van't Hoff equation

$$\frac{dlnK}{dT} = \frac{\Delta H^{o}}{RT^2}$$

Equation 6: van't Hoff form of Arrhenius equation

$$\frac{dlnk}{dT} = \frac{E_a}{RT^2}$$

Equation 7: Arrhenius equation.

$$k = Ae^{-E_a/RT}$$

Using similar transformations as for the van't Hoff equation, the Arrhenius equation can be made into a plot which is used to determine valuable information about the modeled reaction (Equation 8). By plotting the natural log of k (ln(*k*)) versus the inverse of temperature (1/T), an Arrhenius plot can be used to determine the energy of activation for a reaction, assuming the plot gives a straight line, following an Arrhenius behavior (Equation 9) [49, 50]. This requires the same concentration of reagents, both reactants and catalyst, be used for each reaction at the different temperatures [49].

Equation 8: Rearranged Arrhenius equation

$$ln(k) = ln(A) - \frac{E_a}{RT}$$

Equation 9: Determination of energy of activation (E_a) with Arrhenius plot

$$E_a = -slope * R$$

Both *k* and *A* can be determined experimentally for use in the Arrhenius equation. For this work, *k* was determined by ^{1}H-NMR, while A was calculated for a correction factor. In order to calculate A, Equation 8 can be rearranged into Equation 10 and solved via simultaneous equations.

Equation 10: Rearranged Arrhenius equation to solve for ln(A)

$$ln(A) = ln(k) + \frac{E_a}{RT}$$

2.3 Cellulose and Bacterial Cellulose (BC)

2.1 Cellulose

Cellulose is the most abundant organic polymer produced on Earth, since it is the major carbohydrate synthesized for use in plant cell walls [54-57]. Estimates are over 10^{15} kg (over 11 trillion tons) of cellulose is synthesized and destroyed each year by natural sources [55]. Therefore, cellulose has become the target of high impact research in order to best utilize this plentiful, easy to obtain polymer. A form of cellulose known as bacterial cellulose (BC) has been studied in our lab as a potential biomaterial, for both bone and cartilage tissue engineering applications [58-60]. In order to improve the biomaterial properties and extend the applications of BC, surface modifications have been proposed as a method to improve cell adhesion, proliferation, and infiltration depending on cell type and application. This has shown to be effective in multiple published articles, which are discussed in section 2.3. PEG-TECC components could also lead to incorporation of PEG-TECC hydrogel as a potential drug delivery vehicle attached to the surface of BC.

2.2 Synthesis and Physical Properties of BC

BC is cellulose synthesized by bacterial strains such as *Acetobacter, Agroacterium, Pseudomonas, Gluconacetobacter Rhizobium,* and *Sarcina* [54, 61]. BC is a polymer of glucose forming β-1,4- linked glucose with a preferential chair conformation of β-D-glucopyranose. The biochemical pathway for synthesis of BC starts with glucose which is modified through a series of steps to uridine diphosphate glucose (UDP-G). UDP-G is then synthesized into cellulose by the enzyme *cellulose synthase* in between the outer membrane and cytoplasma membrane of BC producing bacterial strains [54]. Because of this β linkage between glucose moieties, the linear polymer chains form with the glucopyranose residues flipped 180^0 relative to each other, forming a repeat group that is cellobiose instead of glucose (Figure 13) [57].

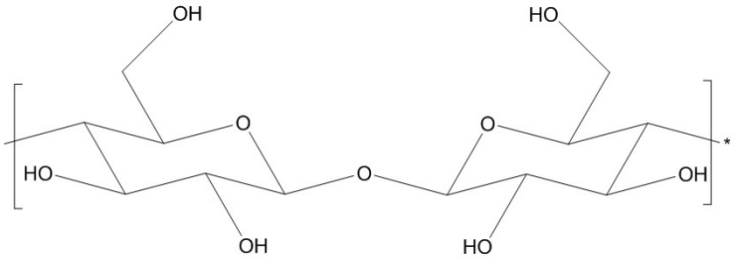

Figure 13: Cellobiose, repeat unit for BC.

The cellulose chains are bundled into ribbons of cellulose microfibrils, which form the crystalline structure of BC [54, 57]. These microfibrils have been shown to have tensile strength comparable to steel [55-57, 61-65]. A recent review of BC showcased some samples that were capable of producing fibers with a tensile strength of 260 MPa and Young's modulus of 16.9 GPa [64], while other articles suggest a theoretical Young's modulus of over 130 GPa [65]. The reason for the incredible strength of the fibers is due to hydrogen bonding in cellulose microfibrils. There is extensive hydrogen bonding that occurs between neighboring glucose residues and parallel chains due to the alternating flip of glucose in the cellobiose repeat unit. There are two distinct forms of hydrogen bonding which occurs in the microfibrils. Intramolecular hydrogen bonding occurs between adjacent hydroxyls and can also be between hydroxyls and the ring oxygen of an adjacent glucose residue. Intermolecular hydrogen bonding only occurs between hydroxyls on parallel chains. However, the extent of hydrogen bonding is not the same for all cellulose and, depending on source, may only undergo one type of hydrogen bonding [57, 66]. The degree of hydrogen bonding determines physical properties, with the hydrogen bonding of BC fitting both types discussed. This gives BC its exceptional mechanical properties, with a percent crystallinity reported to range 70-90% for various types of BC producing bacterial strains and preparation methods [61, 65].

BC is naturally produced as a hydrogel, which is 99% water by weight, consisting of the microfibrils previously discussed [60]. The many benefits of BC over plant cellulose include the previously described high crystallinity, high strength (even when wet), high water absorption, biocompatibility, can be used in both degradable or non-degradable forms, and being free of plant cellulose biogenics that require removal such as lignin, pectin, or hemicellulose [58-60, 62, 67-71]. BC shares some common traits with collagen, giving it the added benefit of being able to mimic the extracellular matrix. Both collagen and cellulose function as the main structural supports, have fibers of similar diameter, and are assembled into polymer chains through biochemical precursors taken from the extracellular environment [62, 70]. Because of these preferential properties, BC hydrogels have seen extensive study for applications involving cell culture and other therapeutic applications which are discussed in section 2.3.

2.3 Applications and Surface Modifications

BC is chemically identical to cellulose found in plants. As discussed in section 2.1, the microfibril crystalline structure making up BC sets it apart from plant cellulose and is the reason it has become a popular and successful target for tissue engineering. As discussed previously, the high strength and biocompatibility of BC are significant for tissue engineering purposes. Applications for BC include vascular implants [67, 72-74], artificial veins due to the ability to be grown into a tubular shape [75], meniscus implants [76], aortic heart valve prosthesis with poly(vinyl alcohol) [77], a scaffold for cartilage repair

[68, 78], bone tissue engineering [59, 79-81] and even use in fuel-cells with palladium [82]. In its naturally occurring form, BC is non-degradable *in-vivo* for humans and animals due to a lack of the required cellulase enzyme [55]. However, through a simple peroxidate oxidation reaction, BC has been shown to form degradable aldehyde linkages but still maintain mechanical stability [60].

Surface modification of BC has also been put forth to improve both mechanical and cellular response to the hydrogel. Cellulose has been modified through the addition of biodegradable polyesters [83], copper catalyzed click chemistry reagents [30, 31, 84, 85], and TECC reagents [86, 87], while BC studies have included surface modification with poly(l-lactic) acid [61, 65], peptides to improve cell adhesion for blood vessel replacements [88], and heterogeneous esterification through organic acids [89]. BC, to the knowledge of the author and advisor, has not been shown to be functionalized with TECC components in as simple of a manner as presented in this work. Previous studies using cellulose films, not BC hydrogels, have shown functionalization with TECC components, requiring silane chemistry [86]. The method provided by this work shows that surface modification of BC can be made as simple as TECC itself. The surface modification presented here required only two steps, which are shown in Figure 14. This approach required only 3 hours of supervision due to elevated temperatures, with most of the reaction time occurring overnight without needing overseeing or multiple washes. BC was modified with 2-chloroethyl acrylate (CEA), which provides reactive acrylate functionalities on the surface of BC for further TECC modification.

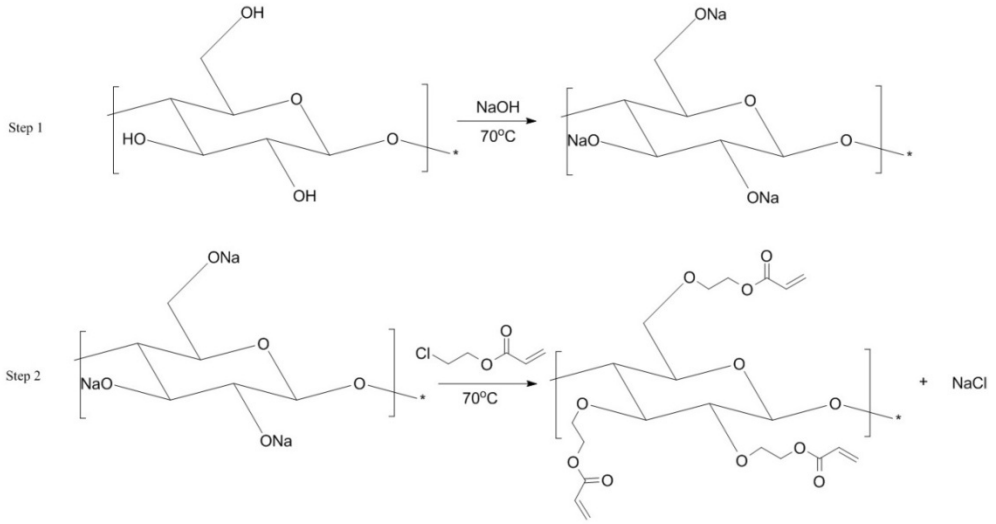

Figure 14: Surface modification of BC with 2-chloroethyl acrylate (CEA).

2.4 Analytical Techniques

The purpose of this section is to provide a brief overview of the techniques used during the course of this work for those readers who are not familiar with the topics. It is not an exhaustive discussion of the techniques, as that is better suited for the textbooks and the other sources cited in this section.

2.4.1 Proton Nuclear Magnetic Resonance (^{1}H-NMR)

^{1}H-NMR spectroscopy has been used to study kinetics for years, with data tables for spectra chemical shifts detailed for most functional groups with available hydrogen(s) to monitor. Isotopes observable by nuclear magnetic resonance (NMR) possess angular momentum, or spin, which generates a magnetic field. A magnetic moment, parallel to the angular momentum vector, can only be detected for atom in which the mass number (A) and atomic number (Z) are both odd, A is odd and Z is even, or A is even and Z is odd. If both A and Z are odd, there will be no magnetic moment, due to equal numbers of opposing spin [90, 91]. This explains why both oxygen and carbon-12 (^{12}C) cannot be detected by NMR [52, 90].

Differences in the local environments, such as being near highly electronegative atoms such as oxygen, lead to deshielding of the hydrogens, pushing their NMR peaks further downfield. The furthest downfield peaks are reserved for carboxylic acid hydrogens, with δ=12 for ^{1}H-NMR while methyl groups (-CH_3) are upfield closer to δ=1 where δ=0 is the position of a reference standard. However, much more information can be extracted from a NMR spectrum other than the position of peaks. This includes peak splitting (also known as coupling), which is determined by the number of neighboring equivalent hydrogens, and integration of the peak giving the number of hydrogens that represent that peak relative to the standard peak [52, 90, 91].

In carbon-13 nuclear magnetic resonance (^{13}C-NMR), an isotope of carbon which contains an extra neutron relative to ^{12}C is able to be detected. However, ^{13}C accounts for only 1.1% of all carbon on Earth, so making a sample which is able to work for both ^{1}H-NMR and ^{13}C-NMR experiments is difficult due the significant difference in sample concentrations needed for both experiments [51, 52, 90, 91].

2.4.2 Quartz Crystal Microbalance with Dissipation (QCM-D)

Another method used to follow the PEG-TECC reaction kinetics was QCM-D. In this section, a brief introduction to the theory of QCM-D and self-assembled monolayers (SAM) is presented to those not familiar with this relatively new technique. During a QCM-D experiment, solutions are passed through a flow chamber in which the response of a gold coated sensor to the molecules in solution is measured. This response requires that molecules bond to either the gold coated sensor or to molecules already bonded to the sensor. The response is measured by the change in frequency and dissipation. For thin ideal films,

there should be no change in dissipation as this is the loss of energy of the film over time. Films which exhibit this behavior can be modeled with the Saubrey model. However, films which are not ideal will show a loss of energy and thus changing dissipation response. The Voigt Viscoelastic model is then used to model films which follow this behavior.

For this experiment, a SAM of 1,10-decane-dithiol (DDT) was first used to cover the gold coated side of the QCM-D sensor. DDT, once bonded to the sensor by a gold-sulfur bond on one end, would leave unreacted thiols at the other. PEG-ACY would then be able to bond to these unreacted thiols so the reaction could be monitored.

Figure 15: 1,10-Decane-dithiol (DDT) used for SAM formation.

Alkanedithiols have been studied extensively for their ability to form SAMs when adhered to gold surfaces in a variety of ways. The success of building the ideal "leaning tower" SAM can be difficult, with problems arising from exposure to air, solvent, chain length, and in the case of dithiols, sulfur-sulfur interactions [92-96]. One issue with alkanedithiols when forming SAMs is the so-called "bridge" form in which both sulfur groups bond to the gold surface, bending over in the middle of the compound and preventing further reactions. Some success for preventing this has been seen by simply extending the hydrocarbon chain separating the two sulfur groups, increasing the hydrophobic interaction between SAM molecules to prevent both sulfur groups from bonding to the surface [95].

QCM-D has been used to show stable formation in many published articles and does this by measuring the frequency and dissipation of the gold sensor as it changes from the initial readings due to adhesion of molecules to the surface [97, 98]. The model used for QCM-D non-ideal films is the Voigt Viscoelastic model. With it come certain assumptions for any numerical analysis. These include complete and homogenous coating of the QCM-D crystal surface, the molecules are attached rigidly, and the film acts as a Newtonian fluid [97].

2.4.3. Bromine Addition to Alkenes for Colorimetric Assay

Most analytical techniques tend to take time and money in order to determine structure or other results. However, a very old technique that is still highly desirable is the colorimetric assay. These are simply visual techniques that require a solution to either change color or remain colored upon the addition of the colorimetric agent. In the case for this work, bromine acted as the colorimetric agent and worked via an addition reaction to confirm surface modification of BC.

Bromine, a dihalide compound, is a red liquid. Bromine, when added to water even in minimal volumes, will change the clear water into a red/yellow solution. However, this can be reversed if the bromine is able to react with a compound in the solution. Once the BC was functionalized with CEA, the carbon-carbon double bond present on the acrylate could serve as the perfect reactive site to remove the red liquid from the solution. Once all alkene groups were saturated with bromine, the solution would again become yellow/red with additional bromine. The reaction of bromine to alkene used in this project is shown in Figure 16. Bromine is known to add to alkenes by an anti-addition mechanism [52, 91].

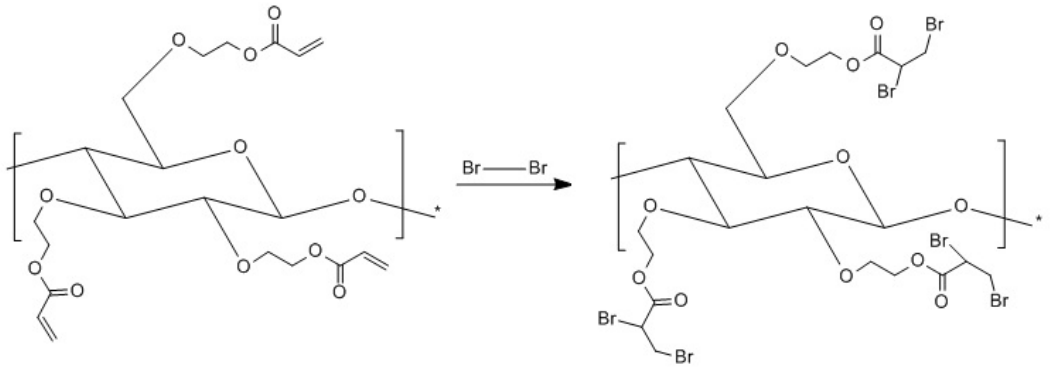

Figure 16: Addition of bromine to CEA modified BC.

2.4.4 Fourier Transform Infrared Spectroscopy-Attenuated Total Reflectance (FTIR-ATR)

Attenuated total reflectance (ATR) is a technique derivative of Fourier transform infrared spectroscopy (FTIR) and follows similar principals. Both FTIR and FTIR-ATR use a low power laser in order to study the functional group composition of samples. FTIR-ATR is a specific form of FTIR in that it can study the surface of thin or thick films, while FTIR is a technique used to study thin films.

During an FTIR-ATR scan, a laser is used to excite molecules and possibly create a change in the dipole moment. The absorption bands present in the FTIR-ATR spectrum corresponds to the functional groups that have undergone changes in their dipole moments. This technique does not affect the charge of the molecules, but the distance between atoms by way of stretching, vibration, bending, or other forms of motion. The infrared beam first enters an ATR crystal where it undergoes total internal reflectance (TIR), making many bounces with the surface of the crystal until exiting. During the internal reflection, an evanescent wave penetrates the sample surface. Samples in close contact with the surface of the crystal can be scanned for surface composition. However, the angle of incidence to the crystals plays a large role in quality of scans, with a

critical angle (Θ_c) that is dependent on the refractive indices of the crystal (n_1) and the sample (n_2) (Equation 11) [56]. The depth of penetration of the evanescent wave can be determined using a simple relationship between the wavelength of the radiation (λ), the refractive indices of the ATR crystal and sample, and the angle of incidence between the ATR crystal and light source (Θ) [99] (Equation 12) .

Equation 11: Critical angle for ATR

$$\theta_c = \sin^{-1} {}^{n_2}/_{n_1}$$

Equation 12: Depth of penetration using ATR

$$D_p = \frac{\lambda}{(2 * \pi * sin^2\,\theta - {}^{n_2}/_{n_1})^{0.5}}$$

2.4.5 Titration

Titration has been used for centuries in order to determine the unknown concentration of an analyte by the addition of a titrant. The titrant is either an acid or base of varying strength, depending on the analyte being studied. In the work presented in this thesis, modified BC had a beginning pH similar to that of a weak acid (pH = 5.5) so a strong base was used as a titrant. The titrant is added to the analyte solution until the reaction is complete, coupling with the discovery of the equivalence point. The equivalence point is the point during the titration experiment in which the titrant and analyte are in equal molar amounts. Visually, the equivalence point is taken as the middle of the sudden change of the titration curve. It can also be determined mathematically by taking the derivative of the curve and finding the maximum value corresponding to the largest change in the slope of the curve. This equivalence point is an ideal point, but what is actually measured is called the end point. This point is the sudden change in properties of solution, which was the pH of the solution for this work. The sudden change in pH comes from a combination of the disappearance of the analyte (due to reaction) or the appearance of an excess of the titrant. The work presented was that of a direct titration, in which titrant was added until the reaction was completed and the upper pH limit was stabilized [51, 100].

CHAPTER 3
METHODS AND MATERIALS

3.1 Kinetics and Energy of Activation (E_a) of PEG-TECC

3.1.1 Materials

PEG-SH and PEG-ACY powders were purchased from Creative PEGworks (Winston Salem, USA). Both had a MW of 1000 Da. ^{1}H-NMR solvent was deuterium oxide (D_2O) (Sigma Aldrich, St. Louis, USA). Two nucleophilic catalysts were used; hexylamine (Fischer Scientific, Hampton, USA) and ethylenediamine (Acros Organics, Geel, Belgium). 4,4-dimethyl-4-silapentane-1-sulfonic acid (DSS) (Acros Organics, Geel, Belgium) was used as the reference peak in ^{1}H-NMR experiments. QCM-D experiments used the SAM molecule DDT (Fisher Scientific, Hampton, USA). DDT provided the reactive thiol group, which reacted with polyethylene glycol diacrylate (PEG-2ACY) (Polysciences, Inc., Warrington, USA) dissolved in DI water. Cleaning chemicals included Contrad 70 (Decon Laboratories Inc., King of Prussia, USA), Hellmanex II (Fisher Scientific, Hampton, USA), 30% hydrogen peroxide (Sigma-Aldrich, St. Louis, USA), and ammonia hydroxide (Fisher Scientific, Hampton, USA).

3.1.2 Methods

3.1.2.1 ^{1}H-NMR Determination of Kinetics and E_a for PEG-TECC

Monofunctional PEG-SH and PEG-ACY were used as received. Separate PEG-SH and PEG-ACY D_2O 10% w/v solutions were made in a glove bag in an inert argon environment. Solutions were then put on ice and left for 30 minutes. Samples were then taken for ^{1}H-NMR testing. ^{1}H-NMR studies were performed on a Liquid State Varian VNMRS 600 MHz (Agilent Technologies, Santa Clara, USA) machine in the laboratory of Dr. Engin Serpersu at the University of Tennessee, Knoxville. PEG-SH and PEG-ACY solutions were mixed together and added to a Shigemi NMR tube, without catalyst to get the blank spectrum of the two components. Without a nucleophilic catalyst the reaction would be unable proceed. The Shigemi tube was subsequently removed from the 600 MHz machine where a nucleophilic catalyst, hexylamine or ethylenediamine, was added in controlled but varying amounts. Multiple experiments were performed in order to determine the optimal catalyst volume for the different temperatures needed to determine the activation energy. The optimal volume of ethylenediamine was then used in order to determine the reaction kinetics at 21, 25, 29, and 32^{0}C. Catalyst volume for kinetic studies was 2.5 µL. Once the catalyst was added, the sample was repeatedly scanned at set time points until the reaction completed. Reported chemical shifts (δ) are in reference to DSS, which was added to the samples in order to provide the zero point and integration reference. The reaction was monitored by decrease in intensity of the thiol hydrogen peak (δ= 4.35) and double bond alkene hydrogen peaks from the

acrylate (δ= 6, 6.25, and 6.5) as the reaction proceeded and is reported quantitatively. The increase in intensity of the CH_2 (δ= 3.0) peak was also observed and is reported only qualitatively due to crowding in the region preventing reliable integration. Reactions were monitored until the thiol and alkene peaks reduced to near-zero. The energy of activation was then determined by plotting reaction rate constants as a function of the inverse of temperature in an Arrhenius plot. Analysis was done using MestReNova® (Mestrelab Research, Escondido, California) and modeling was done with GraphPad Prism 5® software (GraphPad Software, Inc., La Jolla, California).

3.1.2.2 QCM-D

QCM-D crystals were cleaned prior to any experiments to reduce noise levels. All glassware was first cleaned by soaking in 5% Contrad 70 solution overnight, rinsed with DI water, and finally autoclaved at 121^0C for 40 minutes. Crystals were first treated in a UV/Ozone oven for 15 minutes, set a minimum of 5 mm from the bulb by being placed on glass platform. Crystals were then cleaned in a diluted basic piranha solution, 5:1:1 mixture of DI water, 25% ammonia, and 30% hydrogen peroxide heated to 75^0C for 10 minutes. Crystals were then rinsed with DI water, dried with nitrogen and taken for a repeated UV/Ozone treatment. Crystals were then installed in the QCM-D chambers. All flow rates were 100 µl/min for QCM-D experiments, except rinsing steps which were up to 250 µl/min. The dithiol SAM solution, 10 mM DDT in ethanol, was passed first to form a stable SAM surface for further reactions. Once a stabilized SAM layer formed, a water buffer was passed to remove non-adhered SAM molecules. 2PEG-ACY with ethylenediamine catalyst was then passed over the crystal to react with the free –SH molecules from the deposited SAM. Thickness and time measurements were recorded using a Q-Sense E4 machine with QTools® (Q-sense AB, Gothenburg, Sweden). The QCM-D was set to keep the reaction chamber at 21^0C throughout the duration of the experiment to qualitatively compare the reaction time with ^{1}H-NMR results. Upon completion of the experiments, chambers were cleaned by running 2% Hellmanex II in DI water at 250 µl/min for 10 minutes. Modeled data includes 3rd, 5th, and 7th harmonics.

3.2 Surface Modification of BC

3.2.1 Materials

BC was grown by using BC Scramm-Hestrin media and mannitol. BC pellicles were stored in DI water until ready for surface modification. Reaction chemicals included sodium hydroxide pellets (NaOH, Fisher Scientific, Hampton, USA), 2-chloroethyl acrylate (CEA, Sigma Aldrich, St. Louis, USA), bromine reagent (Sigma Aldrich, St. Louis, USA), and hydrochloric acid (HCl, Fisher Scientific, Hampton, USA).

3.2.2 Methods

3.2.2.1 Synthesis of BC

BC was prepared using a previously optimized protocol following the protocols set by Schramm-Hestrin's 1954 article [60, 101]. The strain for BC synthesis was *Gluconacetobacter sucrofermentans*, obtained from the American Type Culture Collection (Manassas, VA, USA) (ATCC 700178). The cellulose was cultivated for 14 days in Schramm-Hestrin media with a sugar source of mannitol. The prepared cellulose was heated at 90^{o}C to kill bacteria and washed with 1% NaOH until absorbance from UV-Vis was less than 0.05. Purified BC was then washed with Millipore water until the solution reached a neutral pH.

3.2.2.2 Surface Modification Reaction and Sample Preparation

Solid pellicles of BC were soaked in 15 ml in DI water for 15 minutes. The effects of surface modification reagent concentration and pH were investigated to determine the extent of modification. Experimental conditions are summarized in Table 2. The pH of the solution was raised with NaOH. For all modifications, the solution with BC pellicles was evacuated with nitrogen and left for 1 hour at 70^{0}C. This initial step was in accordance with previously publish modifications of BC using NaOH [69]. CEA was then added to the solution to achieve the desired concentration, stirred, and covered with aluminum foil for the duration of the reaction. The temperature was raised to 70^{0}C for 2 hours, removed from heat and then left overnight while stirring. BC pellicles were removed from solution, neutralized with 0.1 mM HCl, and washed with DI water. Samples were frozen in 7 ml of DI water and lyophilized for 2 days.

Table 2: BC surface modification sample matrix

Sample Set	*Volume of H_2O (ml)*	*pH*	*Concentration of CEA (mM)*
Control	15	7.0	0
1	15	10	50
2	15	12	200
3	15	12	600

3.2.2.3 Colorimetric Assay

One pellicle from each reaction condition was placed in 5-10 ml of DI water. Bromine was then added drop-wise to each container, in 1 µL drops, until the solution changed color from clear to yellow/red (i.e. bromine saturation). Pictures and video of the color change was recorded using a Droid X ® phone (Motorola Mobility, Inc., Schaumburg, USA).

3.2.2.4 FTIR-ATR

For FTIR-ATR studies, a KRS-5 crystal prism was used in order to detect successful surface modification of BC pellicles. The key absorption band was at

1735 cm^{-1}, corresponding to the carbonyl peak found in the acrylate of the attached molecule .Scans were performed at 50^0 incident to surface of the BC pellicles. Each spectrum was obtained with 1024 co-scans and resolution of 1 cm^{-1}. Scanning and deconvolution was done using Varian FTS – 6000e FTIR equipment with Resolutions Pro FTIR Software® (Agilent Technologies, Santa Clara, California).

3.2.2.5 Titration

Titration experiments were done using a Mettler Toledo SevenMulti pH meter (Mettler-Toledo Inc., Columbus, OH). Lyophilized BC pellicles were soaked in 40ml of DI water, with a stirring bar used to evenly distribute the titrant. After a baseline reading, 0.015 M NaOH was added drop-wise as the titrant for both control and surface modified samples. The pH was recorded as a function of volume of titrant and until an upper baseline was found. Analysis was done using Microsoft Excel ® and MatLab ®. Matlab® was used to determine the equivalence point of both native and modified BC by finding the maximum value for the first derivative of the titration curves as is a common method [100]. The coded program used to determine the equivalence point for both native and modified BC is given in the appendix (Appendix 7)

CHAPTER 4
RESULTS

4.1 PEG-TECC Reaction Studies

4.1.1 ^{1}H-NMR Results

The reaction between PEG-ACY and PEG-SH included two catalysts. First, hexylamine, a commonly used catalyst for the Michael-addition TECC reaction, was used with success when at room temperature or colder. Higher temperatures proved impossible with this catalyst since raising the temperature to 29^0C was enough to prevent the hexylamine from being miscible with the solvent. The catalyst was switched to the infrequently used ethylenediamine for the reported kinetic studies. Initial experiments were performed to determine what catalyst volume could be used at all temperatures to provide reliable scans. From these, 2.5 µL was determined to be the optimal volume and could be used at a wide range of temperatures to allow for proper monitoring of the reaction. Reactions were monitored until peaks related to the thiol and carbon-carbon double bond of the acrylate fell into noise (Figure 17 and Figure 18). Close-ups of the relevant peaks at the beginning (Figure 19) and the end (Figure 21) of the reaction are shown for clarity. Further close-ups of the alkene (Figure 20), thiol (Figure 22), and amine (Figure 22) peaks are also shown, taken from the 21^0C experiments. Alkene peaks (δ = 6, 6.25, and 6.5) and thiol peak (δ = 4.35) stem from the two PEG molecules while the amine peak (δ = 4.28) comes from the ethylenediamine catalyst. Peak positions and characteristics are summarized in Table 3.

Table 3: ^{1}H-NMR PEG-TECC reaction peaks

Relevant Group	*Chemical shift (δ)*	*Splitting*	*Shape*
DSS	0.00	1	Narrow
Amine (-NH_2)	4.28	5	Broad
Thiol (-SH)	4.35	3	Broad
Alkene(-CH=CH_2)	6.00	2	Narrow
Alkene(-CH=CH_2)	6.25	4	Narrow
Alkene(-CH=CH_2)	6.50	2	Narrow

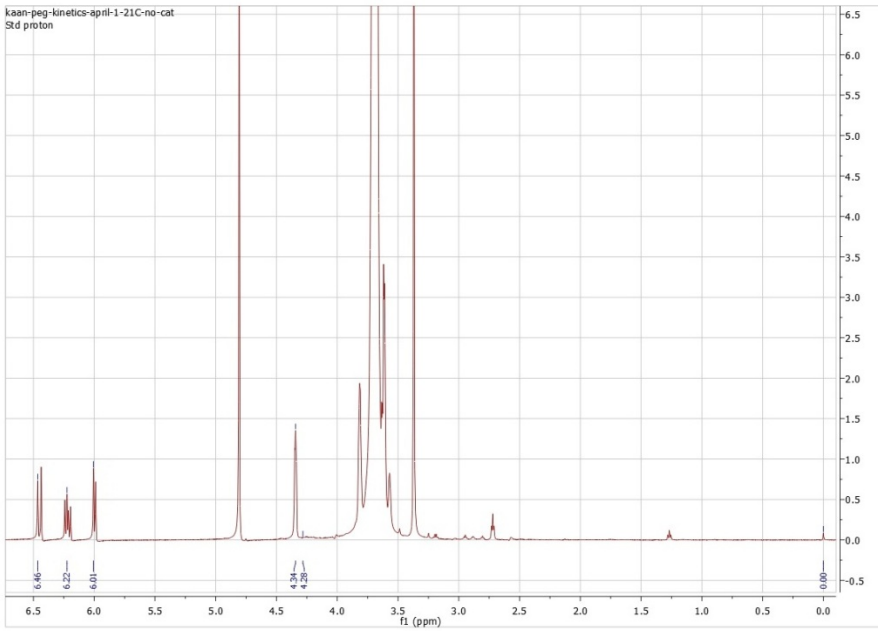

Figure 17: ^{1}H-NMR scan of PEG-TECC reaction without ethylenediamine catalyst at 21^{o}C.

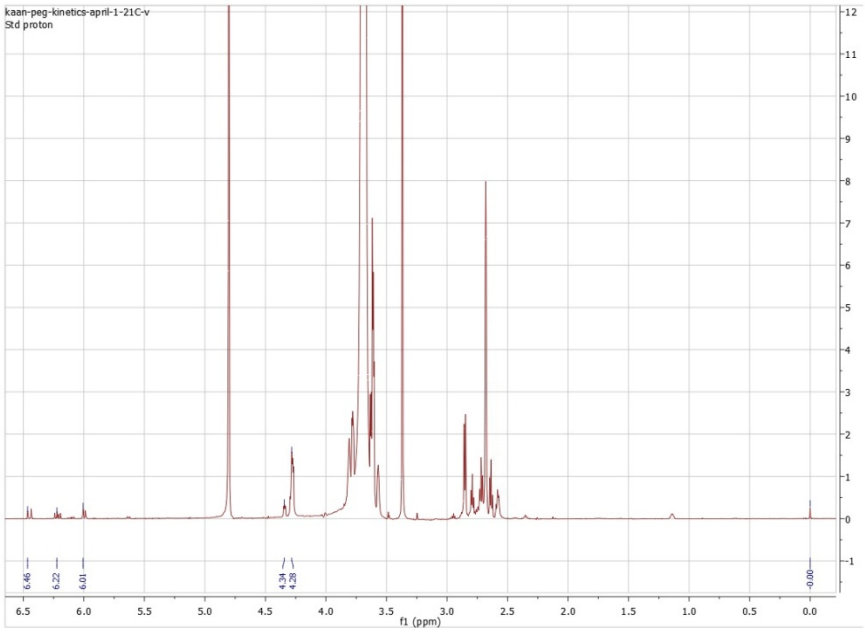

Figure 18: ^{1}H-NMR scan of near complete PEG-TECC reaction with ethylenediamine catalyst at 21^{o}C.

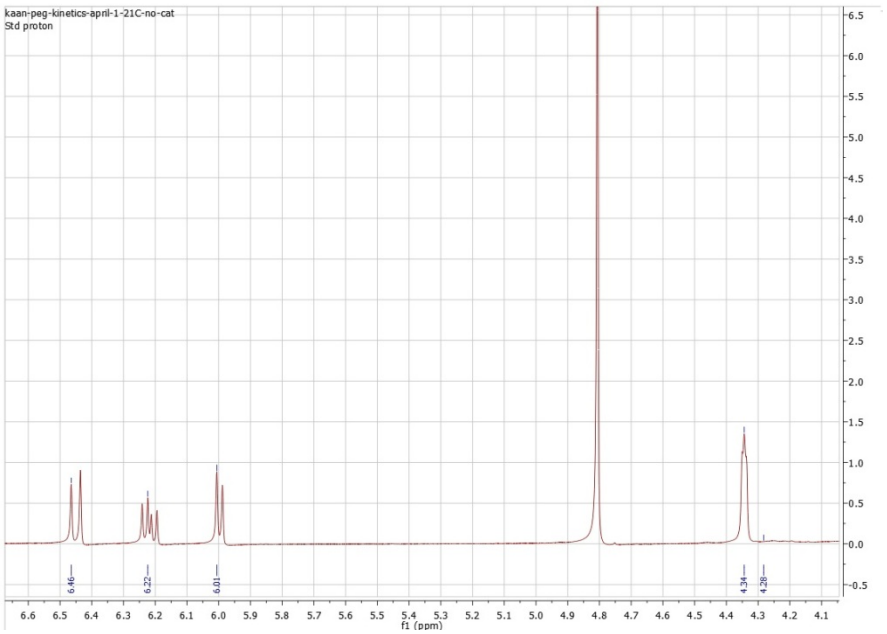

Figure 19: Close-up of ^{1}H-NMR scan of PEG-TECC reaction without ethylenediamine catalyst at 21°C.

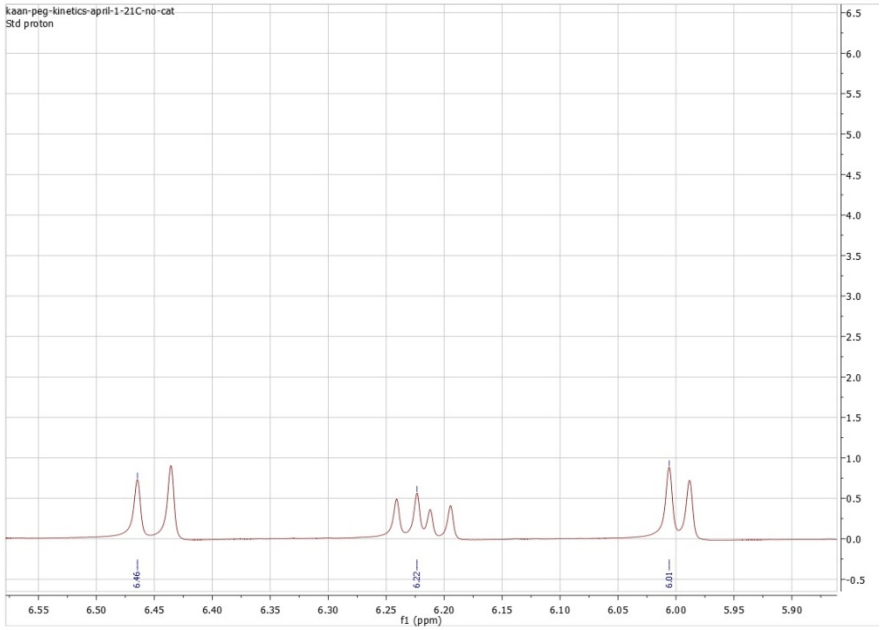

Figure 20: Close-up of the alkene peaks from Figure 19 used for analysis in ^{1}H-NMR kinetic studies.

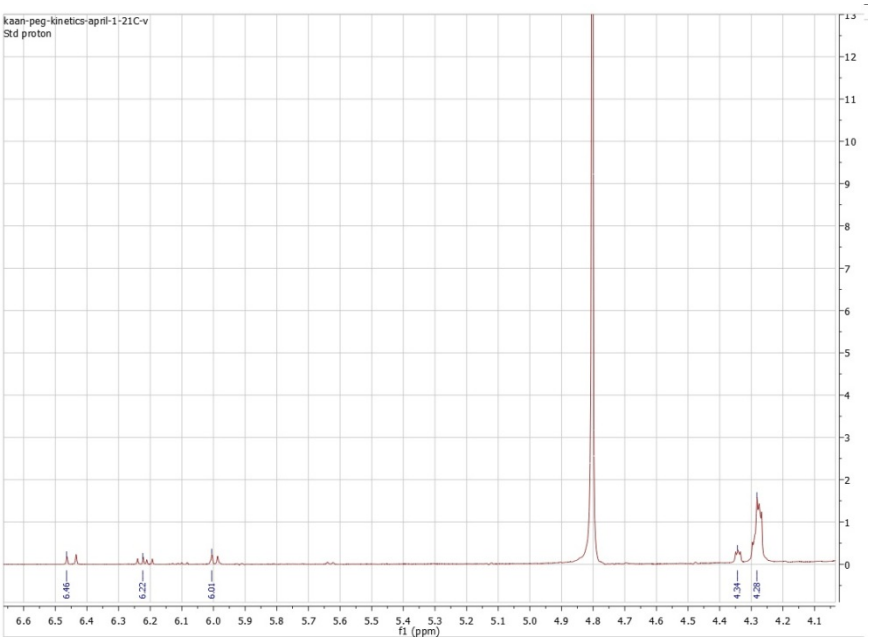

Figure 21: Close-up of ^{1}H-NMR scan near end of PEG-TECC reaction with ethylenediamine catalyst at 21^{o}C.

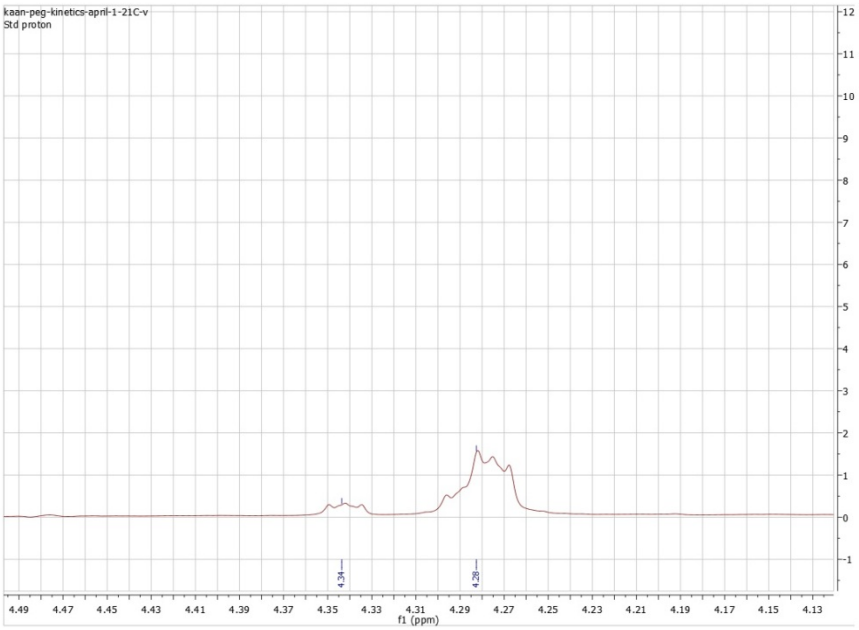

Figure 22: Close-up of thiol (δ = 4.35) and amine (δ = 4.28) peaks seen in Figure 21.

Stacked spectrum for the reaction taking place at 21^{0}C is shown below as an example of the complete data set taken for each temperature (Figure 23 and Figure 24). For both Figure 23 and Figure 24, line 1 is the start of the reaction (no catalyst) and line 23 is the end of the reaction. Similar figures for the reactions at

the three elevated temperatures are given in the appendix (Appendix 1through Appendix 6).

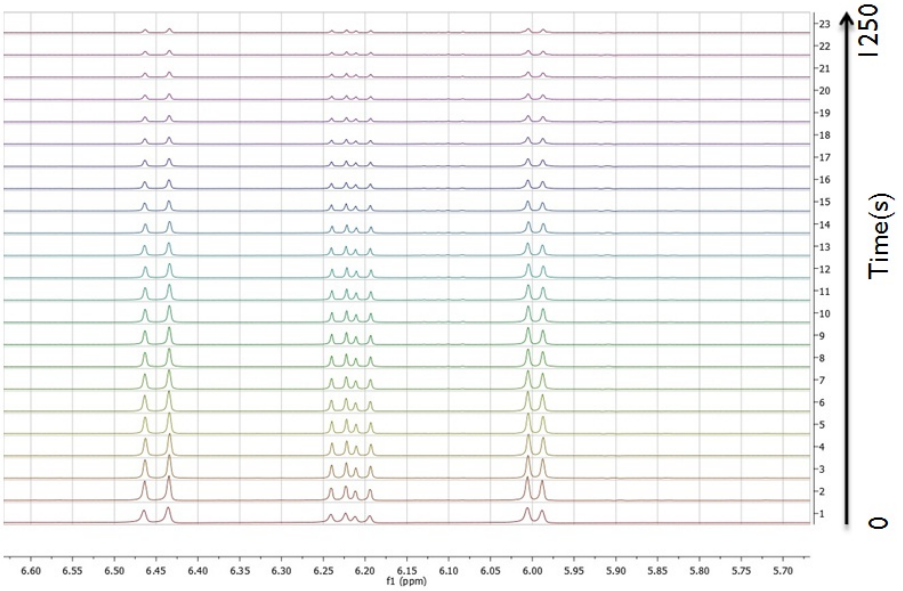

Figure 23: Stacked ^{1}H-NMR spectra for PEG-TECC reaction at 21^{0}C showing alkene intensity drop.

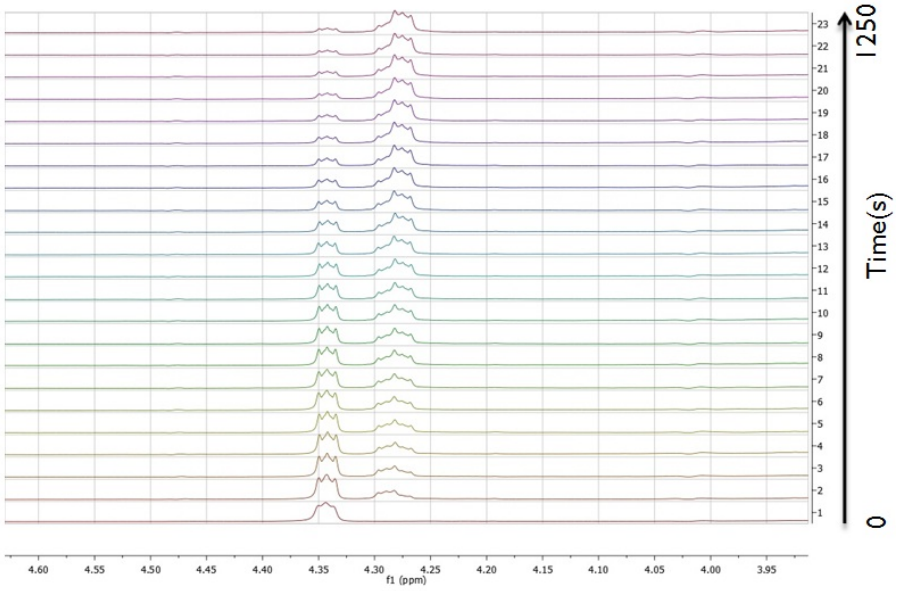

Figure 24: Stacked ^{1}H-NMR spectra for PEG-TECC reaction at 21^{0}C showing thiol intensity drop and appearance of amine peak.

The reaction between PEG-SH and PEG-ACY is reported as the loss of thiol and alkene peak intensity in ^{1}H-NMR scans over the course of the reaction (Figure 25

through Figure 32). An increase in $-CH_2$ peaks, $\delta = 2.5 - 3.0$, can be observed but cannot be determined quantitatively due to crowding in the area. Temperatures over which the reaction was monitored are 21^0C (Figure 25 and Figure 26), 25^0C (Figure 27 and Figure 28), 29^0C (Figure 29 and Figure 30), and 32^0C (Figure 31 and Figure 32). Experiments monitoring the reaction at 37^0C were also tried but due to the reaction completing too quickly for accurate scans is not reported. Reaction rate constants were determined by one-phase model decay and reported in Table 4.

.

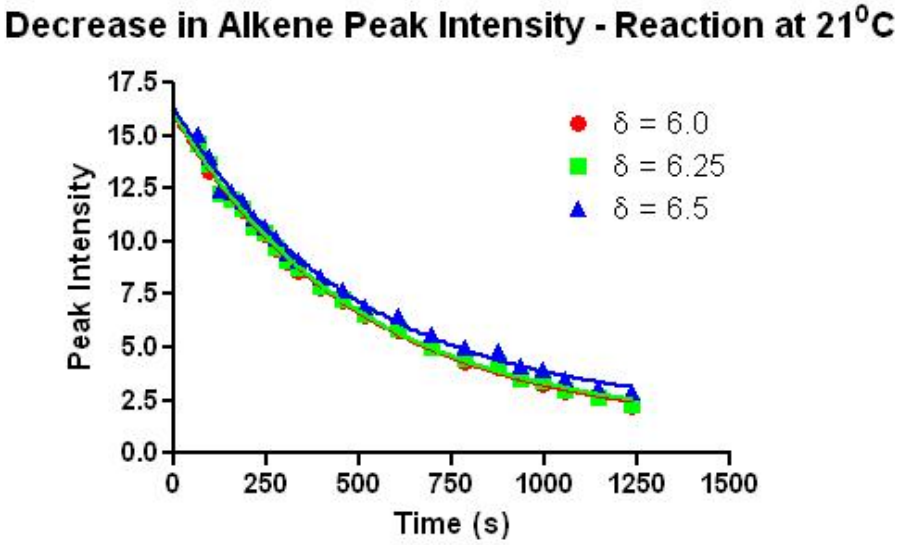

Figure 25: Decrease in alkene ^{1}H-NMR peak intensity during PEG-TECC reaction at 21^oC.

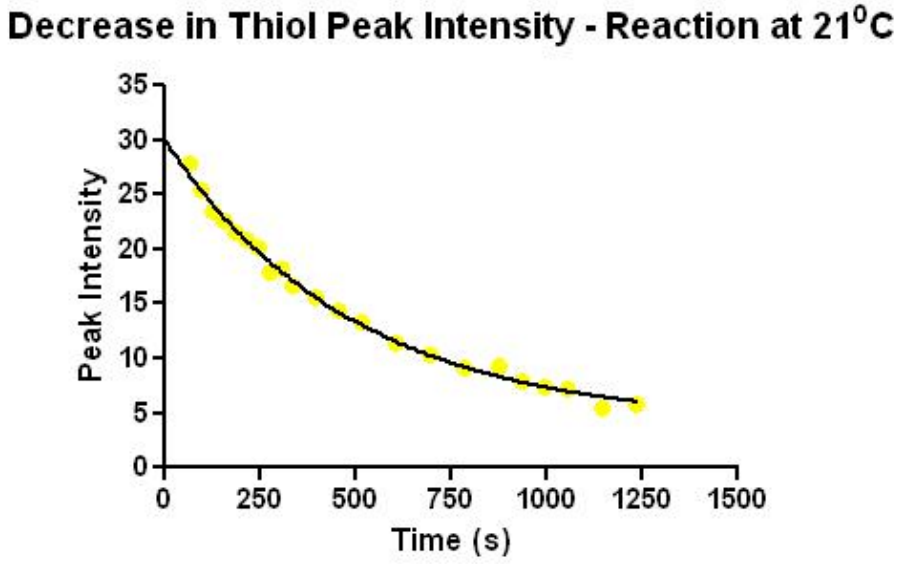

Figure 26: Decrease in thiol ^{1}H-NMR peak intensity during PEG-TECC reaction at 21°C.

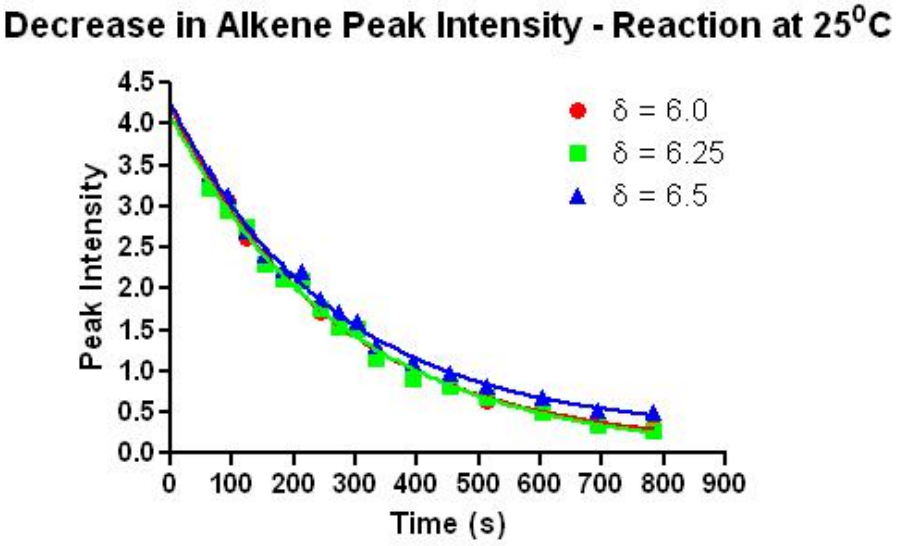

Figure 27: Decrease in alkene ^{1}H-NMR peak intensity during PEG-TECC reaction at 25°C.

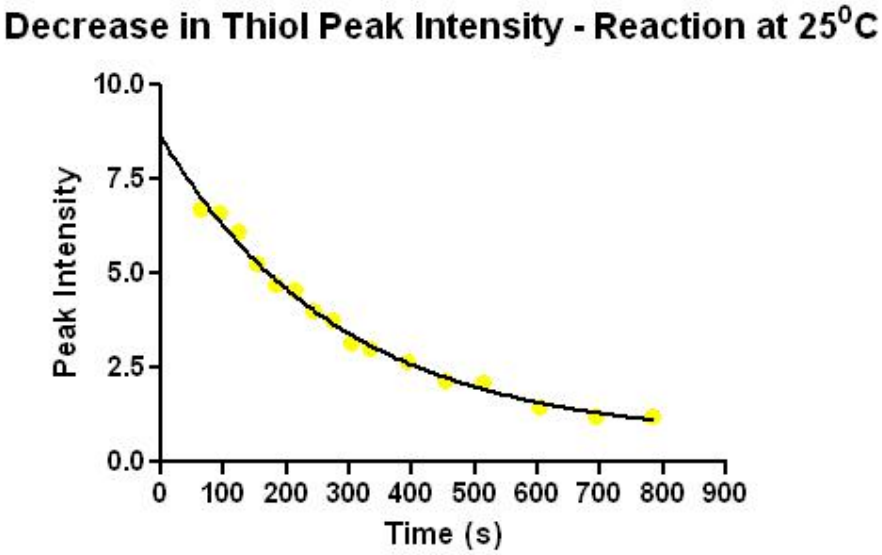

Figure 28: Decrease in thiol ^{1}H-NMR peak intensity during PEG-TECC reaction at 25°C.

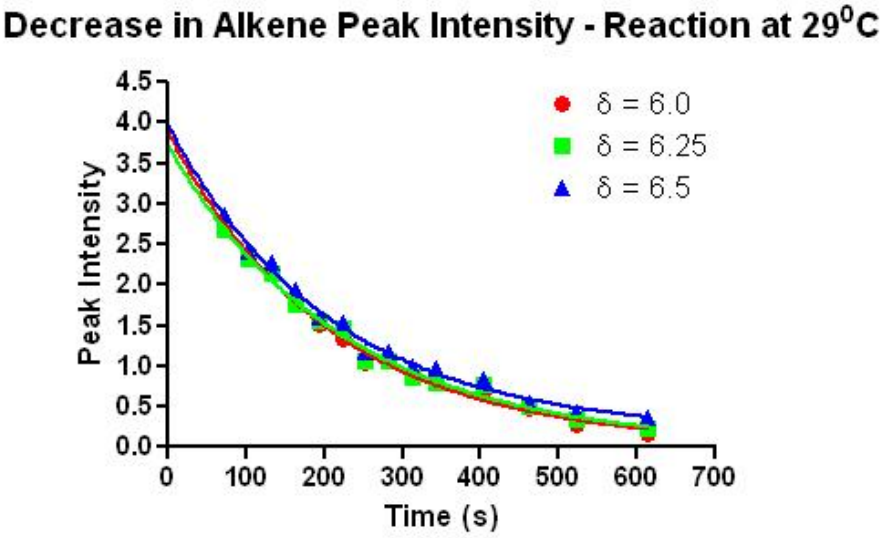

Figure 29: Decrease in alkene ^{1}H-NMR peak intensity during PEG-TECC reaction at 29°C.

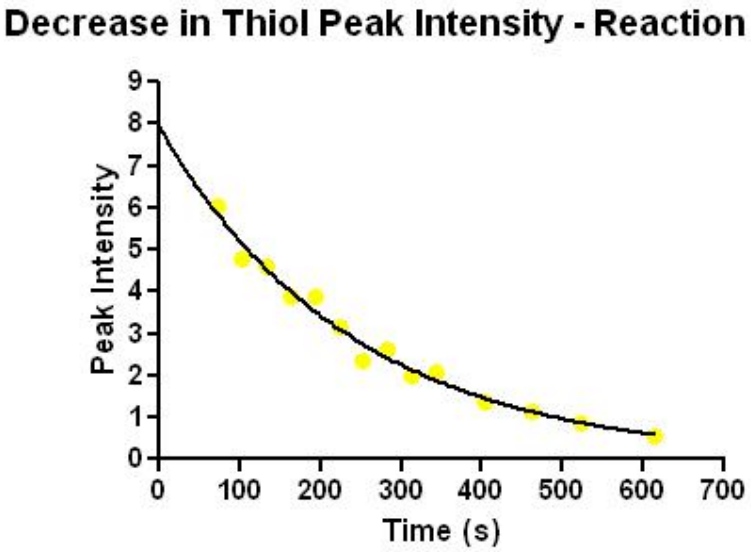

Figure 30: Decrease in thiol ^{1}H-NMR peak intensity during PEG-TECC reaction at 29°C.

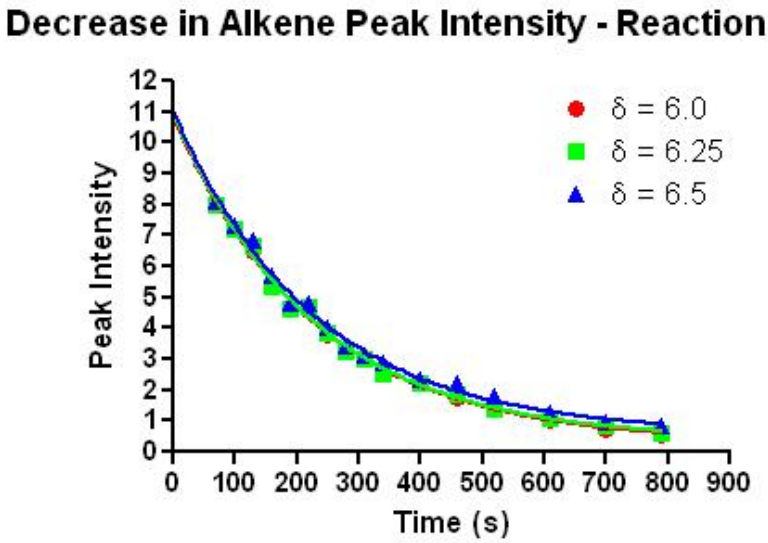

Figure 31: Decrease in alkene ^{1}H-NMR peak intensity during PEG-TECC reaction at 32°C.

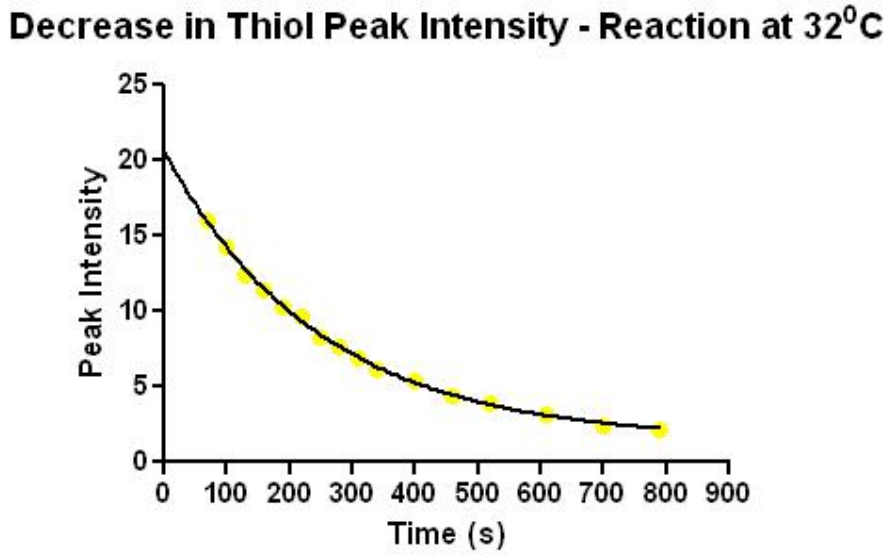

Figure 32: Decrease in thiol ^{1}H-NMR peak intensity during PEG-TECC reaction at 32°C.

Table 4: Rate constants for PEG-TECC reaction at controlled temperatures.

	Temperature (°C)			
	21	25	29	32
Chemical Shift (ppm)	*Rate Constants (k) (s^{-1})*			
4.35	0.00203	0.00349	0.00415	0.00403
6	0.00198	0.00372	0.00478	0.00433
6.25	0.00201	0.00347	0.00446	0.00444
6.5	0.00202	0.00374	0.00477	0.00440

Results from the kinetic experiments provided the rate constants for the reaction at the different temperatures (Table 4). These rate constants are displayed as Arrhenius plots, Figure 33 and Figure 34, with their respective linear regression lines. Figure 33 represents the kinetics for the three alkene peaks followed, while Figure 34 shows the reaction kinetics for the thiol peak.

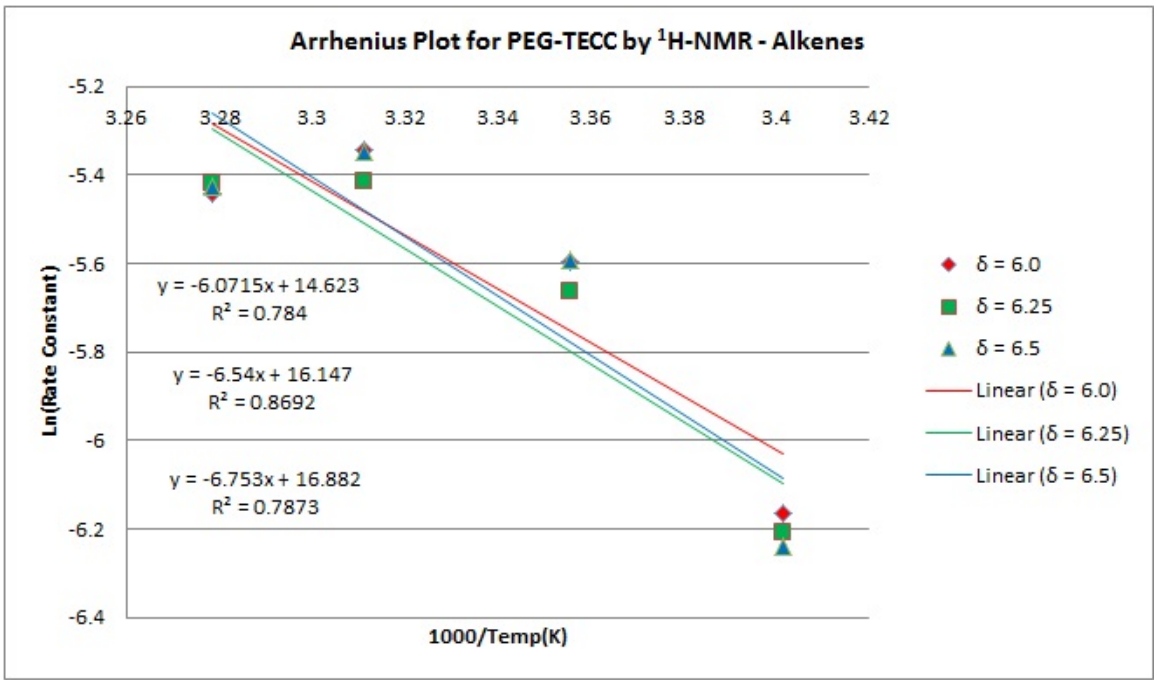

Figure 33: Arrhenius plot for PEG-TECC reaction to determine E_a of reaction using alkene rate constants.

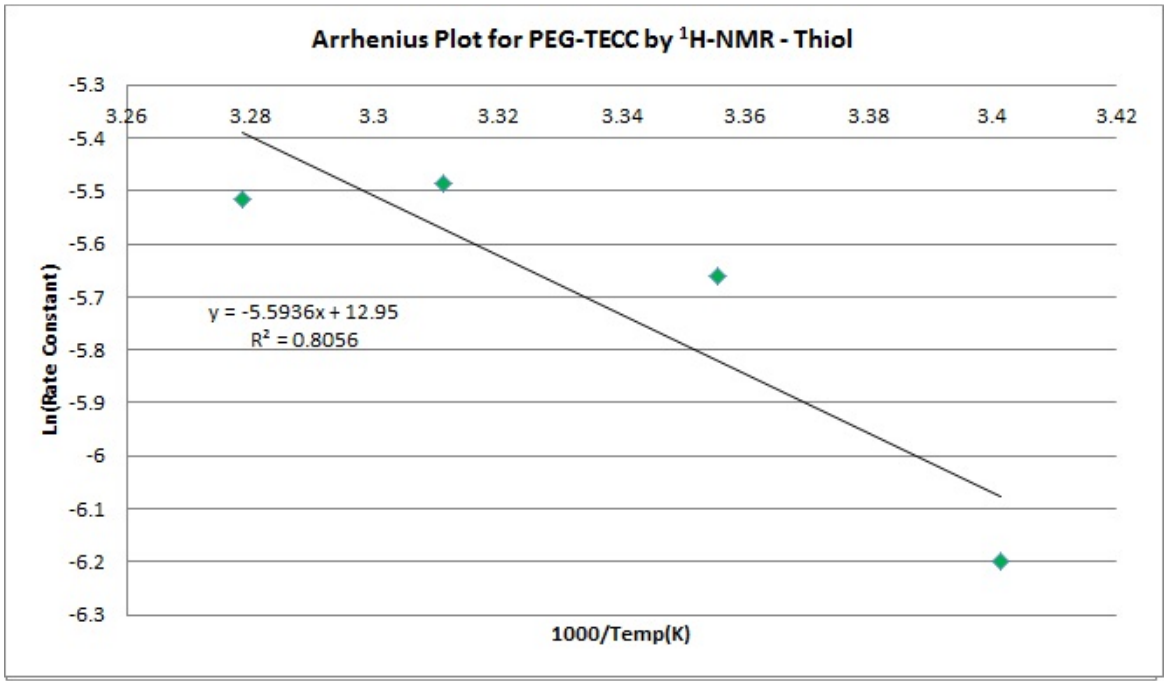

Figure 34: Arrhenius plot for PEG-TECC reaction to determine E_a of reaction using thiol rate constants.

Taking the slopes obtained from Figure 33 and Figure 34 along with the gas constant (R) into Equation 9, the energy of activation (E_a) was determined (Table 5).

Table 5: Energy of activation (E_a) for PEG-TECC reaction

Chemical Shift (ppm)	*Slope of Arrhenius line*	*E_a (kJ/mol)*
4.35	-5.5936	46.5
6.0	-6.072	50.5
6.25	-6.54	54.4
6.5	-6.753	56.1

4.1.2 ^{1}H-NMR Results with Correction Factor

As the temperature is raised, the kinetic rate should increase. However, the results from the 32°C reaction do not exactly match up with the predicted behavior of the reaction. In the data presented, the rate constant for the reaction at 29^{0}C and the reaction at 32^{0}C are almost identical (Table 4). This is thought to be due to elevated temperatures preventing the first steps of the reaction from being observed due to an increase speed of reaction. This speed is a key characteristic of a "click" reaction. These steps were unavoidable missed due to the time between sample preparation and the end of the first scan. To further analyze this data, a correction factor was determined in order to calculate the expected rate constant at 32^{0}C. The reaction follows an Arrhenius behavior (Equation 7), so it follows that by solving for the pre-exponential factor A using only data from 21, 25, and 29^{0}C, the true value for the rate constant at 32^{0}C could be determined.

First, the Arrhenius plots for the alkenes (Figure 35) and thiol (Figure 36) rate constants are shown to showcase the new curves excluding the 32^{0}C reaction data. This highlights a drastic increase in the linear fit (R^2) for all curves. The slopes and y-intercepts of each Arrhenius fit along with the calculated activation energy are shown below in Table 6.

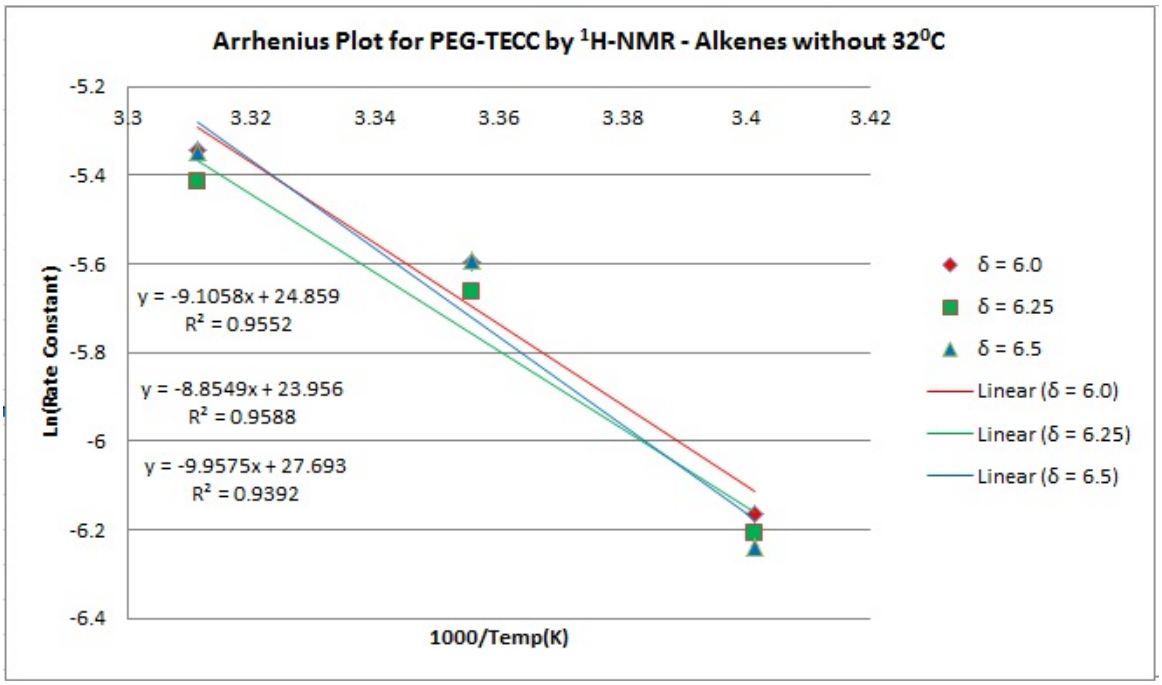

Figure 35: Arrhenius plot for alkenes excluding data from 32^{0}C reaction.

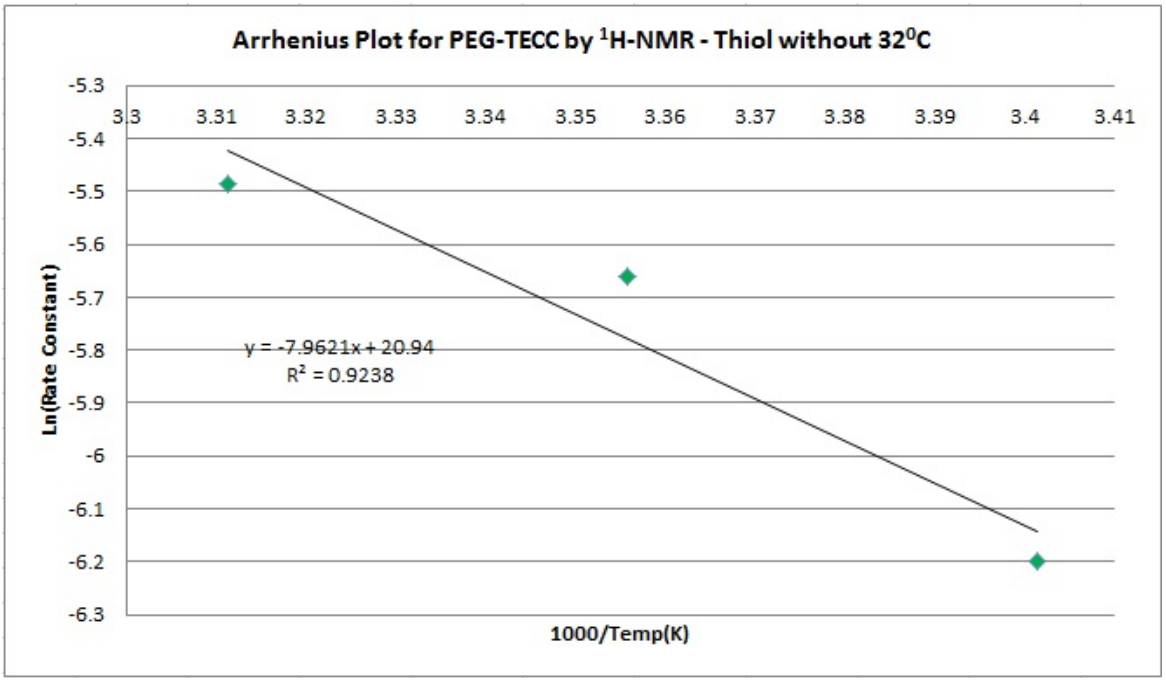

Figure 36: Arrhenius plot for thiol peaks excluding data from 32^{0}C reaction.

Table 6: Arrhenius plot results from correction factor analysis.

Chemical Shift (ppm)	*Slope*	*Intercept*	*Ea (kJ/mol)*
4.35	-9.1058	24.859	66.20
6.0	-8.8549	23.956	75.71
6.25	-9.9575	27.693	73.62
6.5	-7.9621	20.94	82.80

By utilizing Equation 10 and the newly calculated energy of activation from Table 6, it was possible to determine the natural log of A (ln(A)) factor and corrected rate constant (*k*) for the PEG-TECC reaction at 32^0C (Table 7). Ln(A) was determined for each peak at 21, 25, and 29^0C and then averaged to solve for the corrected kinetic rate. A summary of the reaction rates, including the corrected rate for 32^0C is presented in Table 8, with the resulting Arrhenius plots for alkenes peaks (Figure 37) and thiol peak (Figure 38) shown below.

Table 7: Corrected values for ln(A) and k for PEG-TECC reaction at 32^0C.

Chemical Shift (ppm)	*Ln(A)*	*Rate Constant (k) (s^{-1})*
4.35	21.06	0.00650
6	24.86	0.00668
6.25	23.96	0.00626
6.5	27.70	0.00708

Table 8: Corrected rate constants for PEG-TECC reaction

	Temperature (^{o}C)			
	21	25	29	32
Chemical Shift (ppm)	*Rate Constants (k) (s^{-1})*			
4.35	0.00203	0.00349	0.00415	0.00650
6	0.00198	0.00372	0.00478	0.00668
6.25	0.00201	0.00347	0.00446	0.00626
6.5	0.00202	0.00374	0.00477	0.00708

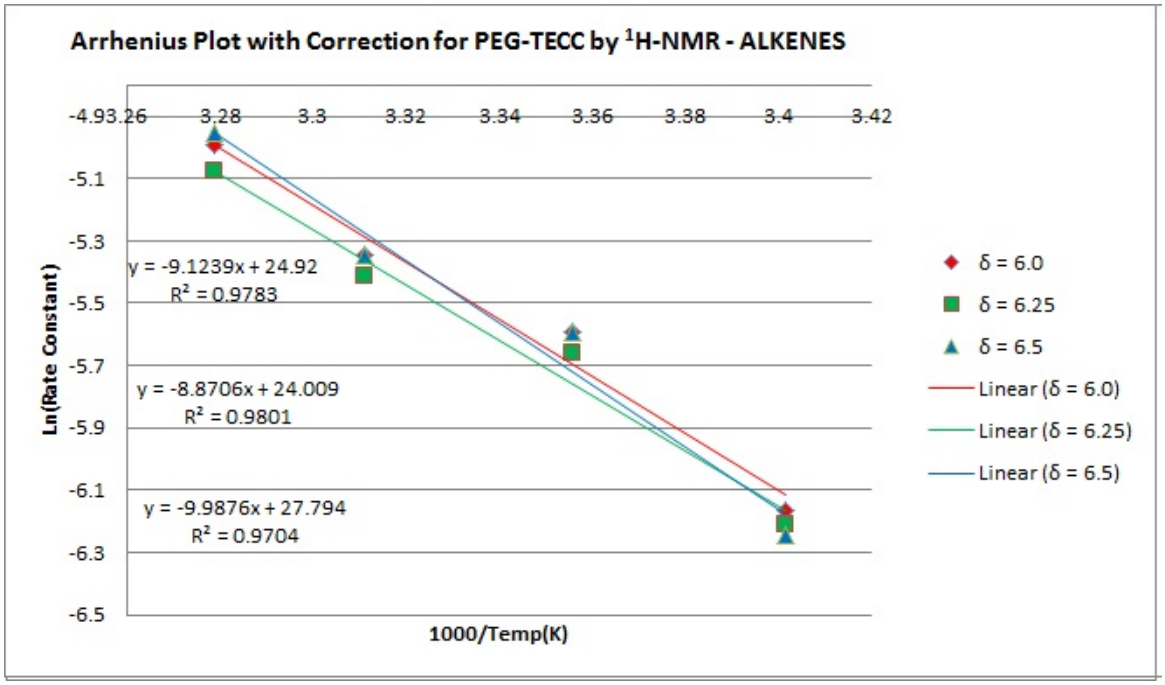

Figure 37: Arrhenius plot of alkene peaks using corrected rate constant for 32^{0}C reaction.

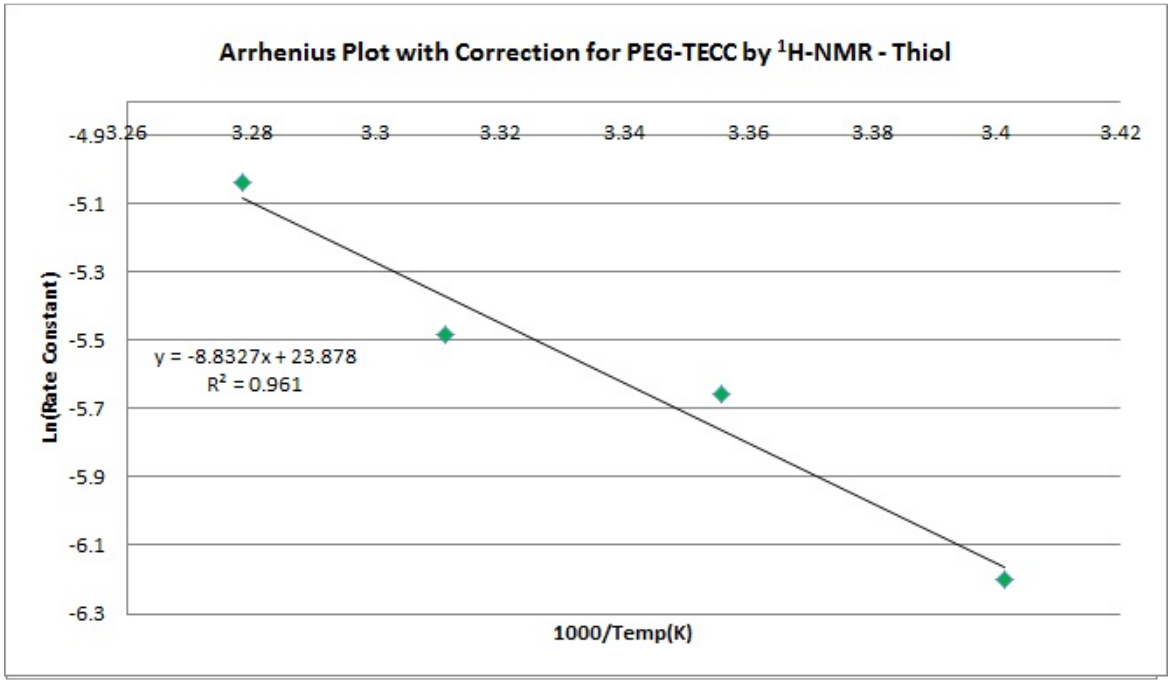

Figure 38: Arrhenius plot of thiol peaks using corrected rate constant for 32^{0}C reaction.

The final corrected energy of activation for the PEG-TECC reaction was then calculated using the same approached that was described previously, in section

4.1.1. Briefly, the slopes of the Arrhenius plots generated with the corrected kinetic rate for the reaction at 32°C, Figure 37 and Figure 38, were used in Equation 9 to determine the final corrected energy of activation (Table 9).

Table 9: Corrected energy of activation (E_a) for PEG-TECC reaction

Chemical Shift (ppm)	*Slope*	*Intercept*	E_a *(kJ/mol)*
4.35	-8.8327	23.878	73.44
6.0	-9.1239	24.92	75.86
6.25	-8.8706	24.009	73.75
6.5	-9.9876	27.794	83.04

4.1.3 QCM-D Results

QCM-D results taken by monitoring the reaction between a dithiol SAM monolayer and 2PEG-ACY are shown below. Figure 39 is the modeled data using QTools ®, with harmonics 5, 7, and 9 used for the model. SAM deposition is shown as the gradual decrease in frequency for 1 hour and 40 minutes before switching to the 2PEG-ACY with ethylenediamine catalyst solution. This data was then used to model the thickness of the molecules adhered to the crystal (Figure 40).

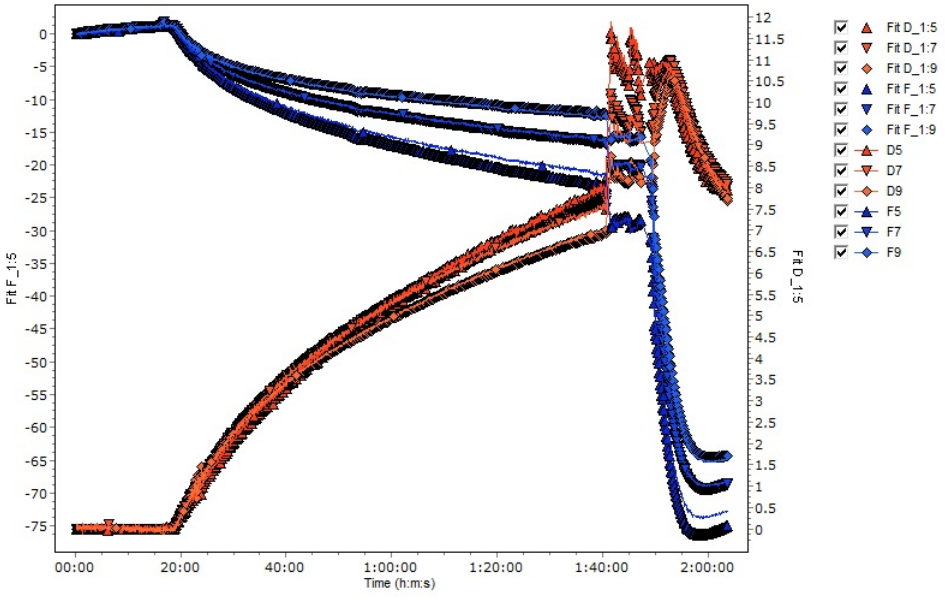

Figure 39: QCM-D monitoring of reaction between -SH and PEG-ACY with ethylenediamine catalyst.

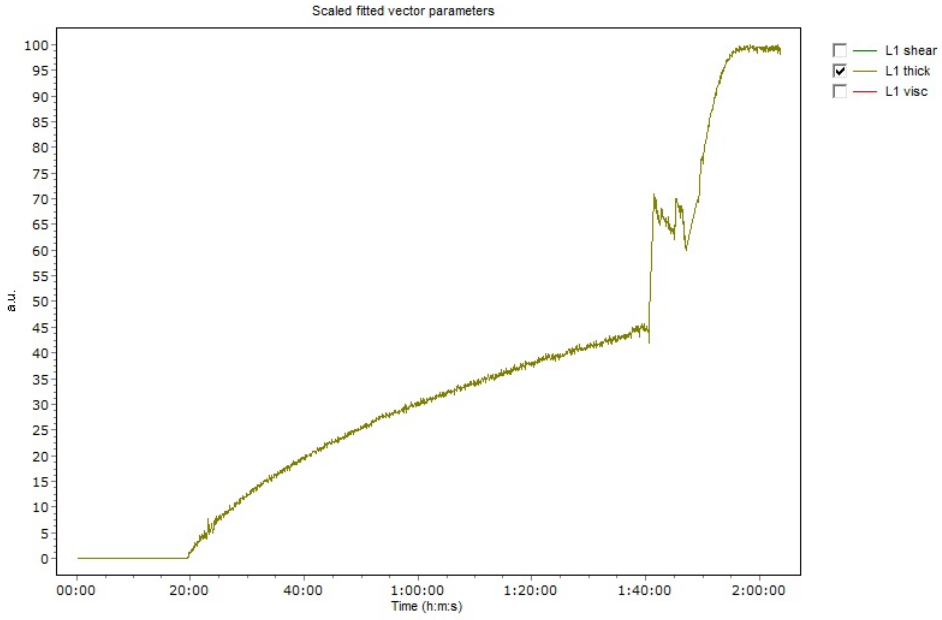

Figure 40: QCM-D modeled thickness for reaction shown in Figure 39

4.2 BC Surface Modification with TECC Components

4.2.1 Colorimetric Results

Control (native) and modified BC pellicles were first tested for the presence of the acrylate group by exposure to a controlled amount of bromine reagent. Bromine, a red liquid, was added in 1 μL amounts to 5-10 ml of water with lyophilized BC samples. Bromine was continuously added until the solution became saturated, i.e. remained colored. This volume was recorded and reported in Table 10. Images were taken after 1 μL of bromine had been added to all samples, shown in Figure 41 and Figure 42.

Table 10: Colorimetric results for BC of different reaction conditions.

Sample Set	*Volume of bromine needed for saturation (μL)*
Control	1
1	1
2	4
3	6

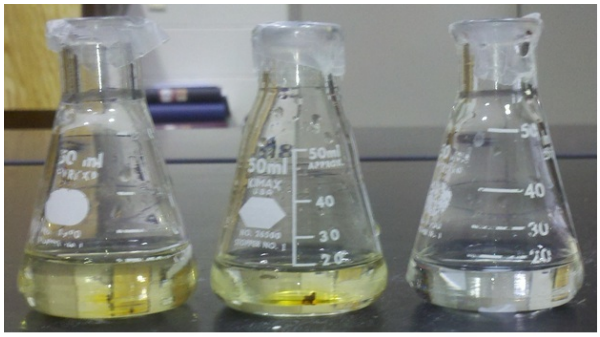

Figure 41: BC samples after addition of 1 μL of bromine. Samples included control BC and BC that underwent reactions 1 and 3.

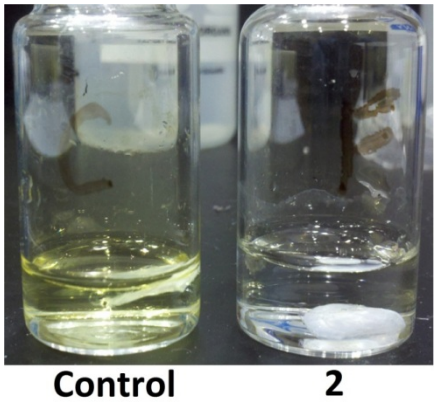

Figure 42: BC samples after addition of 1 μL of bromine. Sample sets were the control BC and BC undergoing reaction 2.

Video of the addition of bromine to the modified BC was taken, with screen captures taken from the video displayed in Figure 43. In Figure 43, the bottle marked C has one pellicle of control BC with 1 μL of bromine already added which turned the solution yellow. The bottle marked F is the modified BC which received 1 μL of bromine, turned yellow but a few seconds later become clear again.

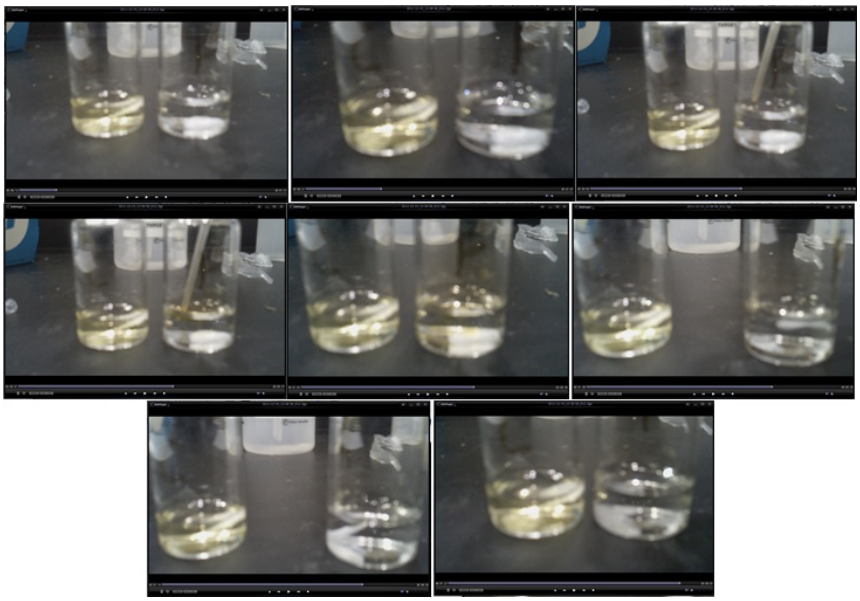

Figure 43: Screen captures from video of addition of bromine to modified BC.

4.2.2. FTIR-ATR Results

FTIR-ATR on native and modified BC was performed at 50^0. This is in reference to the angle of the first mirror prior to the FTIR laser reaching the sample, where decreases in the angle resulted in larger angles of incident with the sample. The FTIR-ATR scans for control BC and modified BC pellicles are shown in Figure 44 and Figure 45, respectively. The spectra taken from the control BC ATR scan was then subtracted from the modified BC scan, shown in Figure 46. Spectra were truncated to remove a noise peak from 2300-2400 $^{-1}$cm, which was related to the air purge of the FTIR system and not the BC pellicles.

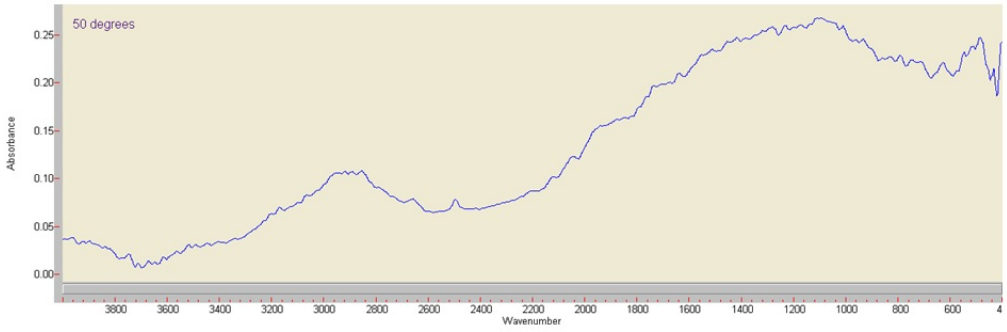

Figure 44: FTIR-ATR scan of native BC at 50^0

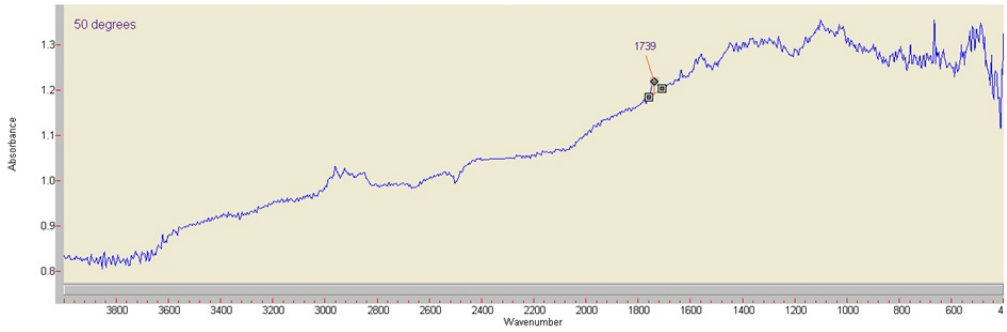

Figure 45: FTIR-ATR scan of modified BC at 50^0

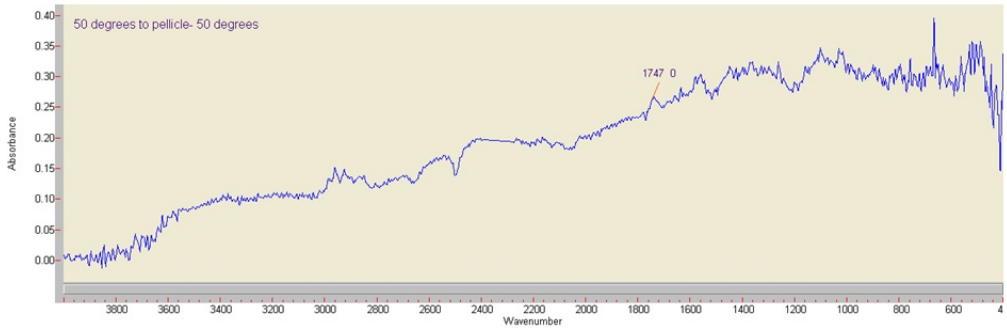

Figure 46: FTIR-ATR scan of native BC subtracted from modified BC at 50^0

4.2.3. Titration Results

Native and modified BC samples were titrated with 0.015 M NaOH in water, while stirring. The results are shown as the pH was measured as a function of the volume of titrant. The native BC titration curve is shown in Figure 47 while the titration curve for modified BC is shown in Figure 48.

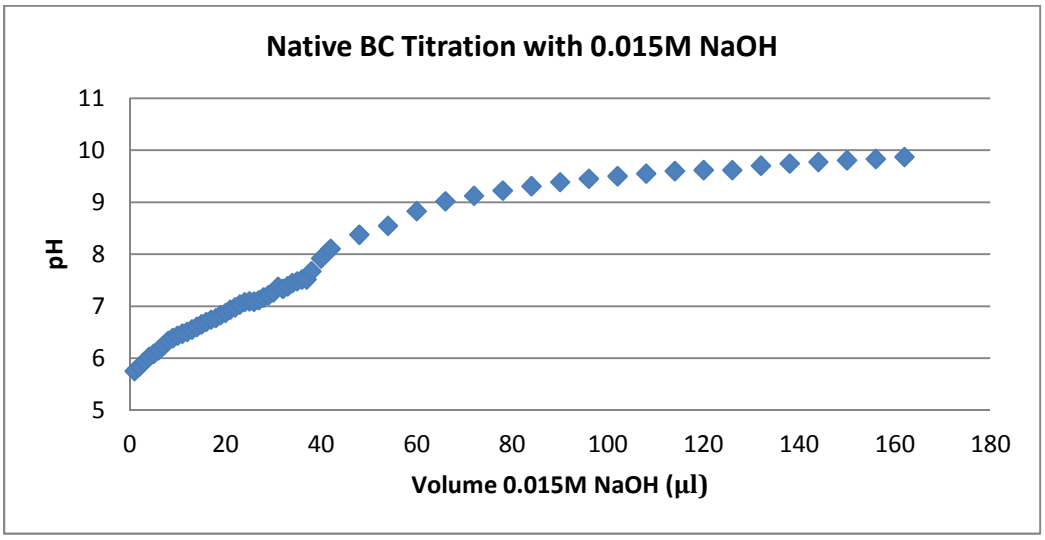

Figure 47: Titration curve for native BC with 0.015M NaOH

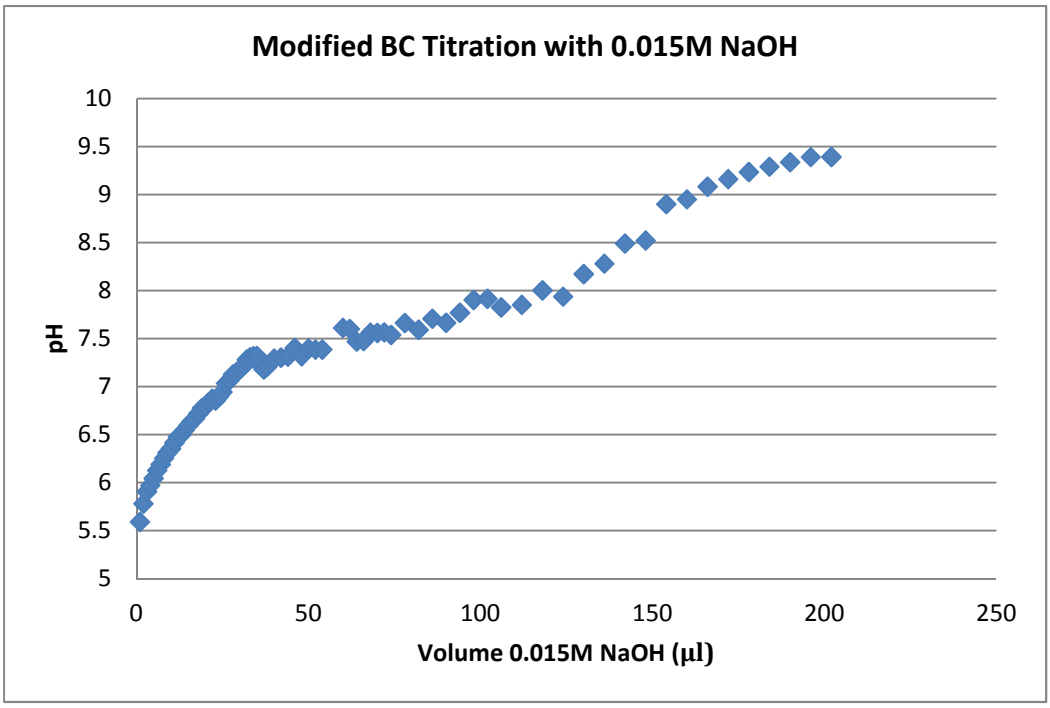

Figure 48: Titration curve for modified BC with 0.015M NaOH

For both native and modified BC, the equivalence point was determined by MatLab ® as the largest slope of the first derivative. The calculated equivalence point and the volume of titrant added to reach the equivalence point is shown in Table 11.

Table 11: Equivalence point and volume of titrant for native and modified BC

BC Type	*Equivalence Point*	*Volume at Equivalence Point (µl)*
Native BC	7.516	37
Modified BC	8.521	148

CHAPTER 5
DISCUSSION

The reaction kinetics for PEG-TECC reaction was monitored by ^{1}H-NMR and confirmation of a similar reaction was done by QCM-D. PEG-TECC ^{1}H-NMR scans fit predictive structure scans. Peaks studied for the hydrogens of the alkenes seen in PEG-ACY were observed at chemical shift δ = 6.0, 6.25, and 6.5. Data on peak splitting in the ^{1}H-NMR scans, displayed in Table 3, shows that the two β-hydrogens on the β-carbon of the alkene gave the expected doublet while the α-hydrogen on the α-carbon gave a doublet of doublet peak. The difference in peak splitting is a result of the different local environments of these three hydrogens [52, 90, 91]. The β-hydrogens closest neighbor to cause splitting is the α-hydrogen, giving them a predictable doublet peak. However, the α-hydrogen has two hydrogen neighbors who are not equivalent. If the two β-hydrogens were equivalent, this would result in a triplet split for the α-hydrogen. The difference between the two β-hydrogens is related to steric hindrance, with one β-hydrogen *cis* to the large PEG backbone, while the other is *cis* to the much smaller α-hydrogen. Thus, the α-hydrogen is two doublet peaks stemming from the two non-equivalent β-hydrogens. The thiol peak, δ = 4.35, was a triplet owing the two equivalent hydrogen neighbors. The amine peak, δ = 4.28, was expected to be a sextet, but due to the broadness of the peak only showed five discernible splits. Both the thiol and amine peaks were broad in nature due to interactions with the solvent, similar to peaks seen for hydroxyl groups [52, 91]. Also like hydroxyl groups, thiol and amine peaks do not exhibit characteristic peaks and have a wide range of peak shifts, depending on the molecule.

The results from both ^{1}H-NMR, Figure 25 through Figure 32, and QCM-D (Figure 39 and Figure 40) show that the reaction was both quick and efficient even at temperatures as low at 21^{0}C. Experiments were also done using hexylamine, which was a fine choice of catalyst at room temperature. However, experiments at the elevated 29 and 32^{0}C temperatures were unsuccessful due to the catalyst no longer dissolving in the heated solution. This is due to the hydrophobic nature of hexylamine by the six carbons found in the backbone, overcoming the hydrogen bonding provided by the amine. Ethylenediamine, a two methyl two amine compound, did not have this problem and was used with great success. Ethylenediamine was miscible in water at both elevated and depressed temperatures and could serve as a successful catalyst. Amine peaks seen in ^{1}H-NMR scans change slightly during the reaction, as expected, due to the reaction mechanism protonating the duel amines to generate the reactive thiolate.

Examining Figure 23 and Figure 24 shows that the alkene peaks and thiol peak can be monitored from the start of the reaction to the end, with the integration from each scan providing the number of hydrogens that had not reacted yet, relative to the reference peak. From this, the reaction kinetics of the PEG-TECC

reaction can be displayed as the loss of hydrogen peak intensity over time. As shown in Figure 25 through Figure 32, all temperatures followed the expected exponential decay behavior. This behavior stems from the change in entropy of the system as the reaction proceeds. As discussed in section 2.2.3, the free energy of the system is dependent on enthalpy, temperature, and entropy [49, 50]. The entropy, in turn, is dependent on the chaotic motion of the molecules. As the reaction continues until completion, fewer molecules are left to react. This gives a lower probability of reactive molecules coupling to form the final product, slowing the reaction rate. The reaction, as by design, decreases the number of molecules as the reaction proceeds, going from two reactants to a single product, which also lowers the entropy of the system [51].

The PEG-TECC reaction taking place at 32^0C required a correction factor due to the incredibly fast nature of the reaction at elevated temperatures. As detailed in section 4.1.2, this was done by solving for the Arrhenius constant, A, at the three lower temperatures, 21, 25, and 29^0C. This determined constant was then used to find the corrected kinetic rate at 32^0C, had the initial seconds of the reaction been successfully monitored. The corrected kinetic rate follows expected behavior, being almost double the rate seen at 25^0C. As the temperature is raised, the velocity of the molecules in solution also raises. The result is an increase in free energy by way of increased entropy by chaotic motion [49, 50]. In fact, experiments at physiologic temperature, 37^0C, were too quick to monitor and obtain reliable data. A significant portion of the initial exponential decay was unable to be obtained by this method and could not be corrected for. While it may seem like a failure, future applications for this work are medical in nature with the purpose of using PEG-TECC being a fast gelling hydrogel. So while the reaction is unable to be monitored at physiologic temperature for energy of activation determination, PEG-TECC is ideal for situations requiring expedient reaction speeds and predictable products at physiologic temperatures.

The energy of activation was determined independently from data from the α-hydrogen, two β-hydrogens, and the thiol hydrogen. The determined energies of activation are similar to values determined for the Cu(I) catalyzed azide-alkyne reaction and the free radical TECC reaction [39, 102-104]. Using the Arrhenius relationship and the discussed correction factor, a final Arrhenius plot of the kinetic rate as a function of temperature, Figure 37 and Figure 38, was used to determine the energy of activation for PEG-TECC. The energy of activation was determined to be about to be between 73.4 and 83 kJ/mol, depending on the particular hydrogen studied. Work by Liang et al. showed that the energy of activation for acrylate substituents used to crosslink poly(2,6-dimethyl-1,4-phenylene oxide) (PPO) increased as the substituent on the acrylate gained additional carbons, comparing methyl and ethyl substituents. This increase in energy of activation was attributed to greater steric hindrance and resistance for bond rotation due to the larger substituent [105]. However, inspection of Table 9,

shows that three of the four calculated energies of activation are very close together, 73.44-75.86, with the energy of activation for δ = 6.5 much larger at 83 kJ/mol. This variation shown by the δ = 6.5 hydrogen is thought to be a result of the difference in local environment. As discussed with peak splitting, the two β-hydrogens are not equivalent with one of the β-hydrogens sterically hindered by being *cis* to the PEG backbone. This increased steric hindrance may have an unexpected effect on ^{1}H-NMR peak intensity during the course of the reaction.

QCM-D studies were used as an alternative method to confirm behavior seen in ^{1}H-NMR studies. The results from QCM-D, Figure 39 and Figure 40, agreed with ^{1}H-NMR results and showed that the reaction between PEG-ACY and available thiol groups does indeed meet the requirement for TECC to be a fast and efficient reaction. As shown in Figure 40, the buildup of the SAM monolayer took one hour and forty minutes of continuous monitoring, while the reaction between the thiol and PEG-ACY only took 20 minutes. The QCM-D was done at 21^{0}C, with this reaction time almost matching the reaction time when studied at the same temperature by ^{1}H-NMR, Figure 25 and Figure 26, which was 20.8 minutes. However, due to the assumptions discussed in section 2.4.2, numerical analysis for the reaction was not performed. This is due to the unknown distribution of the SAM layer and the PEG-ACY inability to act as a Newtonian fluid since polymers exhibit non-Newtonian behavior [1, 2]. This method was useful, however, in providing evidence that the reaction monitored by ^{1}H-NMR was accurate. The slight difference in reaction time when comparing the reactions followed by QCM-D and ^{1}H-NMR reaction are due to the different thiol molecules in their respective reactions, both in terms of structure and concentration of available thiols. If done at the same concentration as the ^{1}H-NMR experiments, it is expected that the PEG-SH would exhibit a faster reaction time than DDT due to the slight acidity of the thiol-hydrogen in PEG-SH from the neighboring oxygen atom [48].

The modification of BC followed the philosophy of TECC, aiming for an inexpensive, simple to do, and effective way to modify the surface of BC. This was done to allow future cell and medical applications to take advantage of BC and PEG-TECC. By modifying the surface of BC with a Michael-addition TECC starting point of an acrylate, future modification can then be easily done by simply introducing a compound with a reactive thiol. This also avoids the need for generating free radicals or using harmful azides, either *in-vitro* or *in-vivo.* Results from colorimetric studies (Figure 41 through Figure 42), FTIR-ATR (Figure 44 through Figure 46), and titration (Figure 47 and Figure 48) showed that the BC was successfully modified.

Colorimetric assays are quick and easy visual experiments that can be used to prevent needless wastes of time. For this work, bromine was added drop-wise to lyophilized BC in water until bromine saturation for the solution occurred and a

red/yellow color was visible. For native BC, there are no reactive sites available to the bromine without the addition of an acid or other catalyst [52]. As such, water with native BC, when exposed to bromine immediately colored red/yellow and remain colored (Figure 41 and Figure 42).

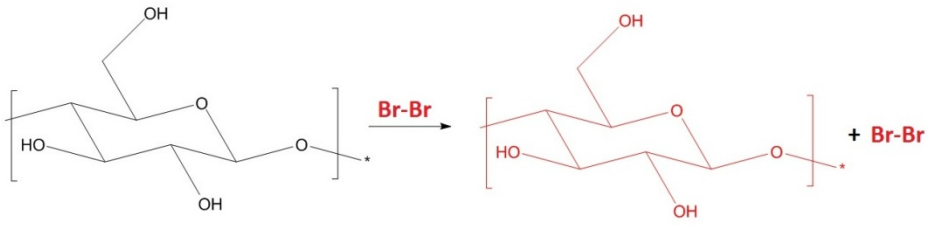

Figure 49: Coloring of native BC as a result of exposure to bromine.

Water with BC that has been modified with acrylates had reactive sites available for bromine, as discussed in section 2.4.3. The alkene present on the modified BC served as the reactive site for the added bromine. Thus, as expected, water with surface modified BC was able to remove bromine from solution, removing any color which was initially present upon addition of bromine (Figure 16, Figure 41, and Figure 42). As shown in Figure 43, this discoloration dissipated and the water turned clear after a few seconds due to the bromine being removed from solution by an addition reaction to the carbon-carbon double bond present on modified BC. This behavior continued until bromine was added in a significant enough volume to saturate the available alkenes. Once saturated, the solution remained colored due to saturation of all available reaction sites on the modified BC. This experiment was invaluable, as it was completed in less than five minutes, while other characterization techniques took a few hours to generate viable results. Thus BC could be tested for modification quickly, before moving on to the more involved FTIR-ATR and titration experiments. Interestingly, BC which had been modified at pH = 10 did not show any reaction to the bromine, suggesting the BC was not modified. This agrees with the reaction portrayed in Figure 14, as the first step is the deprotonation of hydroxyl groups [69]. Increasing the pH to 12 resulted in the successful modification of BC (Figure 41). This also provided evidence that the CEA solution was not imbedded in the BC hydrogel during modification but had been linked to the surface of BC undergoing reactions 2 and 3. If CEA had been imbedded in the hydrogel, BC pellicles modified at pH 10 and 50 mM CEA should have reacted with the added bromine in a similar fashion as BC modified at pH 12 with higher concentrations of CEA.

FTIR-ATR was done on both native and modified BC. The refractive index for native BC has been reported to be between 1.56 – 1.60 [106]. However, this index can decrease by acetylation of the BC surface to as low as 1.47 [106]. This change in refractive index will change the critical angle (Equation 11) that must be exceeded for FTIR-ATR to accurately detect the surface modification. The

minimum angle, assuming an index of refraction of 1.47, was 38^0, while the angle for native BC was calculated to be 42.5^0. For this reason, FTIR-ATR scans were done at 50^0 so both native and modified BC could be scanned at the same angle. The peak of interest is the carbonyl peak, found at 1735 cm^{-1}, which should only be present in modified BC as native BC has no carbonyls to absorb this wavelength. Subtracting the native BC from the modified BC shows the carbonyl peak clearly (Figure 46). This, along with the successful colorimetric experiments showing presence of the alkene, suggests the CEA modification group had been successfully attached to the BC surface.

The final technique used to show successful modification of BC was titration, with two key data points obtained from this technique. The first being the clear change in the equivalence point between native and modified BC, owing to the presence of the acrylate on modified BC. This can be coupled to the other key data point, the volume of titrant needed to reach equivalence. For native BC, only 37 μL of NaOH was needed to reach equivalence. Modification of BC with CEA more than tripled this volume to 148 μL. On native BC, NaOH added drop-wise to the solution will not deprotonate the hydroxyl groups. This is agreed by the fact that attempts at modifying BC at pH = 10 were unsuccessful. The increase of equivalence point and volume needed to reach this point for the modified BC is due to the presence of the ester on CEA. The ester group on modified BC can react with the NaOH by base hydrolysis to form a carboxylate ion and an alcohol [52] (Figure 50).

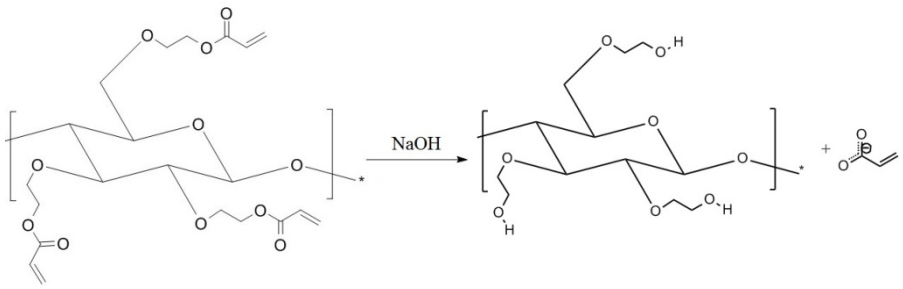

Figure 50: Products as a result of titration of modified BC with NaOH

The three characterization techniques used to determine successful modification of BC can now be combined. The data provided suggest the presence of an alkene, from the colorimetric assay, an ester carbonyl, from FTIR-ATR, and an ester, from titration. All three of these groups are present on the CEA molecule used to modify the BC surface and furthermore is available for reaction. The acrylate group is shown to be available for further reactions, since different moieties of the acrylate reacted with bromine and NaOH titrant. Modified BC with CEA provides an acrylate which is available for TECC reactions by way of Michael-addition with PEG-SH.

CHAPTER 6
CONCLUSIONS AND FUTURE WORK

This work has been the compilation of three years of intense polymer study. While the project itself has not always been the main project, the skills, knowledge, and experience during the time has made this work possible. This work concludes that reactions between PEG-SH and PEG-ACY do in fact follow TECC rules, has an energy of activation around 74 kJ/mol, and can be successfully monitored by both ^{1}H-NMR and QCM-D. In turn, the philosophy behind TECC was what drove the need for a simple and effective way to modify the surface of BC to make it available for future PEG-TECC applications. This work has shown that the modification of BC can be as simple as TECC itself, with just as much success. Future suggest work by our group would include cell culture studies on modified and native BC, the encapsulation of a drug into a PEG-TECC hydrogel functionalized to the surface of BC by degradable links for drug delivery, the inclusion of non-degradable acrylates for applications requiring stable hydrolysis resistant hydrogels [107], and the inclusion of surface peptides attached to BC via TECC to modulate stem cell differentiation.

LIST OF REFERENCES

1. Odian, G., *Principles of Polymerization*. 4th ed. 2004, New York; Chichester: Wiley.
2. Callister, W.D., *Materials Science and Engineering : An Introduction*. 7th ed. 2007, New York: John Wiley & Sons.
3. Ratner, B.D., *Biomaterials Science : An Introduction to Materials in Medicine*. 2nd ed. 2004, Amsterdam; Boston: Elsevier Academic Press.
4. Harris, J.M., *Poly(ethylene glycol) Chemistry : Biotechnical and Biomedical Applications*. 1st ed. 1992, New York: Plenum Press.
5. Slaughter, B.V., et al., *Hydrogels in Regenerative Medicine.* Advanced Materials, 2009. **21**(32-33): p. 3307-3329.
6. Mather, M.L. and P.E. Tomlins, *Hydrogels in regenerative medicine: towards understanding structure-function relationships.* Regenerative Medicine, 2010. **5**(5): p. 809-821.
7. van de Wetering, P., et al., *Poly(ethylene glycol) hydrogels formed by conjugate addition with controllable swelling, degradation, and release of pharmaceutically active proteins.* Journal of Controlled Release, 2005. **102**(3): p. 619-627.
8. Elbert, D.L., et al., *Protein delivery from materials formed by self-selective conjugate addition reactions.* Journal of Controlled Release, 2001. **76**(1-2): p. 11-25.
9. Lin, C.C. and K.S. Anseth, *PEG Hydrogels for the Controlled Release of Biomolecules in Regenerative Medicine.* Pharmaceutical Research, 2009. **26**(3): p. 631-643.
10. Schoenmakers, R.G., et al., *The effect of the linker on the hydrolysis rate of drug-linked ester bonds.* Journal of Controlled Release, 2004. **95**(2): p. 291-300.
11. Gunn, J.W., S.D. Turner, and B.K. Mann, *Adhesive and mechanical properties of hydrogels influence neurite extension.* Journal of Biomedical Materials Research Part A, 2005. **72A**(1): p. 91-97.
12. Scott, R., L. Marquardt, and R.K. Willits, *Characterization of poly(ethylene glycol) gels with added collagen for neural tissue engineering.* Journal of Biomedical Materials Research Part A, 2010. **93A**(3): p. 817-823.
13. Kulbokaite, R., et al., *N-PEG'ylation of chitosan via "click chemistry" reactions.* Reactive & Functional Polymers, 2009. **69**(10): p. 771-778.
14. Lin, C.C., A. Raza, and H. Shih, *PEG hydrogels formed by thiol-ene photo-click chemistry and their effect on the formation and recovery of insulin-secreting cell spheroids.* Biomaterials, 2011. **32**(36): p. 9685-9695.
15. Fernandez-Megia, E., J. Correa, and R. Riguera, *"Clickable" PEG-dendritic block copolymers.* Biomacromolecules, 2006. **7**(11): p. 3104-3111.
16. Dong, Y.X., et al., *"One-step" Preparation of Thiol-Ene Clickable PEG-Based Thermoresponsive Hyperbranched Copolymer for In Situ Crosslinking Hybrid Hydrogel.* Macromolecular Rapid Communications, 2012. **33**(2): p. 120-126.
17. Cabral, J. and S.C. Moratti, *Hydrogels for biomedical applications.* Future Medicinal Chemistry, 2011. **3**(15): p. 1877-1888.

18. Kolb, H.C., M.G. Finn, and K.B. Sharpless, *Click chemistry: Diverse chemical function from a few good reactions.* Angewandte Chemie-International Edition, 2001. **40**(11): p. 2004-+.
19. Kolb, H.C. and K.B. Sharpless, *The growing impact of click chemistry on drug discovery.* Drug Discovery Today, 2003. **8**(24): p. 1128-1137.
20. Zhao, Z.D., et al., *"Click Chemistry" and Its Growing Applications in Biomedical Field.* Progress in Chemistry, 2010. **22**(2-3): p. 417-426.
21. Crescenzi, V., et al., *Novel hydrogels via click chemistry: Synthesis and potential biomedical applications.* Biomacromolecules, 2007. **8**(6): p. 1844-1850.
22. Hein, C.D., X.M. Liu, and D. Wang, *Click chemistry, a powerful tool for pharmaceutical sciences.* Pharmaceutical Research, 2008. **25**(10): p. 2216-2230.
23. Agalave, S.G., S.R. Maujan, and V.S. Pore, *Click Chemistry: 1,2,3-Triazoles as Pharmacophores.* Chemistry-an Asian Journal, 2011. **6**(10): p. 2696-2718.
24. Zhang, Y.H., et al., *An inexpensive fluorescent labeling protocol for bioactive natural products utilizing Cu(I)-catalyzed Huisgen reaction.* Tetrahedron, 2007. **63**(29): p. 6813-6821.
25. Zhan, W.H., et al., *Photovoltaic properties of new cyanine-naphthalimide dyads synthesized by 'Click' chemistry.* Tetrahedron Letters, 2007. **48**(14): p. 2461-2465.
26. Hong, J.A., Q.A. Luo, and B.K. Shah, *Catalyst- and Solvent-Free "Click" Chemistry: A Facile Approach to Obtain Cross-Linked Biopolymers from Soybean Oil.* Biomacromolecules, 2010. **11**(11): p. 2960-2965.
27. Mansfeld, U., et al., *Clickable initiators, monomers and polymers in controlled radical polymerizations - a prospective combination in polymer science.* Polymer Chemistry, 2010. **1**(10): p. 1560-1598.
28. Bock, V.D., H. Hiemstra, and J.H. van Maarseveen, *Cu-I-catalyzed alkyne-azide "click" cycloadditions from a mechanistic and synthetic perspective.* European Journal of Organic Chemistry, 2006(1): p. 51-68.
29. van Dijk, M., et al., *Synthesis and Applications of Biomedical and Pharmaceutical Polymers via Click Chemistry Methodologies.* Bioconjugate Chemistry, 2009. **20**(11): p. 2001-2016.
30. Krouit, M., J. Bras, and M.N. Belgacem, *Cellulose surface grafting with polycaprolactone by heterogeneous click-chemistry.* European Polymer Journal, 2008. **44**(12): p. 4074-4081.
31. Hafren, J., W.B. Zou, and A. Cordova, *Heterogeneous 'organoclick' derivatization of polysaccharides.* Macromolecular Rapid Communications, 2006. **27**(16): p. 1362-1366.
32. Lowe, A.B. and M.A. Harvison, *Thiol-Based 'Click' Chemistries in Polymer Synthesis and Modification.* Australian Journal of Chemistry, 2010. **63**(8): p. 1251-1266.
33. Hoyle, C.E. and C.N. Bowman, *Thiol-Ene Click Chemistry.* Angewandte Chemie-International Edition, 2010. **49**(9): p. 1540-1573.
34. Hoyle, C.E., T.Y. Lee, and T. Roper, *Thiol-enes: Chemistry of the past with promise for the future.* Journal of Polymer Science Part a-Polymer Chemistry, 2004. **42**(21): p. 5301-5338.

35. Lowe, A.B., *Thiol-ene "click" reactions and recent applications in polymer and materials synthesis.* Polymer Chemistry, 2010. **1**(1): p. 17-36.
36. Kade, M.J., D.J. Burke, and C.J. Hawker, *The Power of Thiol-ene Chemistry.* Journal of Polymer Science Part a-Polymer Chemistry, 2010. **48**(4): p. 743-750.
37. Killops, K.L., L.M. Campos, and C.J. Hawker, *Robust, efficient, and orthogonal synthesis of dendrimers via thiol-ene "Click" chemistry.* Journal of the American Chemical Society, 2008. **130**(15): p. 5062-+.
38. Uygun, M., M.A. Tasdelen, and Y. Yagci, *Influence of Type of Initiation on Thiol-Ene "Click" Chemistry.* Macromolecular Chemistry and Physics, 2010. **211**(1): p. 103-110.
39. Shin, J., et al., *Physical and chemical modifications of thiol-ene networks to control activation energy of enthalpy relaxation.* Polymer, 2009. **50**(26): p. 6281-6286.
40. Cook, W.D., et al., *Thermal polymerization of thiol-ene network-forming systems.* Polymer International, 2007. **56**(12): p. 1572-1579.
41. Cook, W.D., et al., *Photopolymerization kinetics, photorheology and photoplasticity of thiol-ene-allylic sulfide networks.* Polymer International, 2008. **57**(3): p. 469-478.
42. Lowe, A.B., C.E. Hoyle, and C.N. Bowman, *Thiol-yne click chemistry: A powerful and versatile methodology for materials synthesis.* Journal of Materials Chemistry, 2010. **20**(23): p. 4745-4750.
43. Movassagh, B. and P. Shaygan, *Michael addition of thiols to alpha,beta-unsaturated carbonyl compounds under solvent-free conditions.* Arkivoc, 2006: p. 130-137.
44. Meciarova, M., S. Toma, and P. Kotrusz, *Michael addition of thiols to alpha-enones in ionic liquids with and without organocatalysts.* Organic & Biomolecular Chemistry, 2006. **4**(7): p. 1420-1424.
45. Meciarova, M. and S. Toma, *Michael addition of thiols to alpha-enones: Is any catalyst necessary?* Letters in Organic Chemistry, 2006. **3**(10): p. 794-797.
46. Heggli, M., et al., *Michael-type addition as a tool for surface functionalization.* Bioconjugate Chemistry, 2003. **14**(5): p. 967-973.
47. Li, G.Z., et al., *Investigation into thiol-(meth)acrylate Michael addition reactions using amine and phosphine catalysts.* Polymer Chemistry, 2010. **1**(8): p. 1196-1204.
48. Chan, J.W., et al., *Nucleophile-Initiated Thiol-Michael Reactions: Effect of Organocatalyst, Thiol, and Ene.* Macromolecules, 2010. **43**(15): p. 6381-6388.
49. Dill, K.A. and S. Bromberg, *Molecular Driving Forces : Statistical Thermodynamics in Chemistry and Biology*. 1st ed. 2003, New York: Garland Science.
50. Chang, R., *Physical Chemistry with Applications to Biological Systems*. 2nd ed. 1981, New York; London: Macmillan Pub. Co. ; Collier Macmillan Publishers.
51. Hill, J.W., *General Chemistry*. 4th ed. 2005, Upper Saddle River, N.J.: Pearson/Prentice Hall.

52. Carey, F.A., *Organic Chemistry*. 7th ed. 2008, Boston, Mass.; Montreal: McGraw-Hill Higher Education.
53. Smith, J.M. and H.C. Van Ness, *Introduction to chemical engineering thermodynamics*. 2nd ed. 1959, New York: McGraw-Hill.
54. Jonas, R. and L.F. Farah, *Production and application of microbial cellulose.* Polymer Degradation and Stability, 1998. **59**(1-3): p. 101-106.
55. Berg, J.M., et al., *Biochemistry*. 5th ed. 2002, New York: W.H. Freeman.
56. Solomon, E.P., L.R. Berg, and D.W. Martin, *Biology*. 7th ed. 2006, Belmont, CA: Brooks/Cole Thomson Learning.
57. Clarke, A.J., *Biodegradation of Cellulose : Enzymology and Biotechnology*. 1st ed. 1997, Lancaster, Pa.: Technomic Publishing Company.
58. Hutchens, S.A., et al., *An Exopolysaccharide Nanofiber Composite for Biomedical Applications.* Aatcc Review, 2009. **9**(12): p. 40-45.
59. Hutchens, S.A., et al., *Biomimetic synthesis of calcium-deficient hydroxyapatite in a natural hydrogel.* Biomaterials, 2006. **27**(26): p. 4661-4670.
60. Hutchens, S.A., et al., *A resorbable calcium-deficient hydroxyapatite hydrogel composite for osseous regeneration.* Cellulose, 2009. **16**(5): p. 887-898.
61. Quero, F., et al., *Optimization of the Mechanical Performance of Bacterial Cellulose/Poly(L-lactic) Acid Composites.* Acs Applied Materials & Interfaces, 2010. **2**(1): p. 321-330.
62. Alberts, B., *Molecular Biology of the Cell*. 5th ed. 2008, New York: Garland Science.
63. Kovalenko, V.I., *Crystalline cellulose: structure and hydrogen bonds.* Russian Chemical Reviews, 2010. **79**(3): p. 231-241.
64. Iguchi, M., S. Yamanaka, and A. Budhiono, *Bacterial cellulose - a masterpiece of nature's arts.* Journal of Materials Science, 2000. **35**(2): p. 261-270.
65. Lee, K.Y., J.J. Blaker, and A. Bismarck, *Surface functionalisation of bacterial cellulose as the route to produce green polylactide nanocomposites with improved properties.* Composites Science and Technology, 2009. **69**(15-16): p. 2724-2733.
66. Roy, D., et al., *Cellulose modification by polymer grafting: a review.* Chemical Society Reviews, 2009. **38**(7): p. 2046-2064.
67. Klemm, D., et al., *Bacterial synthesized cellulose - artificial blood vessels for microsurgery.* Progress in Polymer Science, 2001. **26**(9): p. 1561-1603.
68. Svensson, A., et al., *Bacterial cellulose as a potential scaffold for tissue engineering of cartilage.* Biomaterials, 2005. **26**(4): p. 419-431.
69. Watanabe, K., et al., *A NEW BACTERIAL CELLULOSE SUBSTRATE FOR MAMMALIAN-CELL CULTURE - A NEW BACTERIAL CELLULOSE SUBSTRATE.* Cytotechnology, 1993. **13**(2): p. 107-114.
70. Petersen, N. and P. Gatenholm, *Bacterial cellulose-based materials and medical devices: current state and perspectives.* Applied Microbiology and Biotechnology, 2011. **91**(5): p. 1277-1286.
71. Helenius, G., et al., *In vivo biocompatibility of bacterial cellulose.* Journal of Biomedical Materials Research Part A, 2006. **76A**(2): p. 431-438.

72. Schumann, D.A., et al., *Artificial vascular implants from bacterial cellulose: preliminary results of small arterial substitutes.* Cellulose, 2009. **16**(5): p. 877-885.
73. Backdahl, H., et al., *Mechanical properties of bacterial cellulose and interactions with smooth muscle cells.* Biomaterials, 2006. **27**(9): p. 2141-2149.
74. Fink, H., et al., *An in vitro study of blood compatibility of vascular grafts made of bacterial cellulose in comparison with conventionally-used graft materials.* Journal of Biomedical Materials Research Part A, 2011. **97A**(1): p. 52-58.
75. Ciechanska, D., et al., *Biosynthesis of Modified Bacterial Cellulose in a Tubular Form.* Fibres & Textiles in Eastern Europe, 2010. **18**(5): p. 98-104.
76. Bodin, A., et al., *Bacterial cellulose as a potential meniscus implant.* Journal of Tissue Engineering and Regenerative Medicine, 2007. **1**(5): p. 406-408.
77. Mohammadi, H., et al., *Design and simulation of a poly(vinyl alcohol)-bacterial cellulose nanocomposite mechanical aortic heart valve prosthesis.* Proceedings of the Institution of Mechanical Engineers Part H-Journal of Engineering in Medicine, 2009. **223**(H6): p. 697-711.
78. Andersson, J., et al., *Behavior of human chondrocytes in engineered porous bacterial cellulose scaffolds.* Journal of Biomedical Materials Research Part A, 2010. **94A**(4): p. 1124-1132.
79. Fang, B., et al., *Proliferation and Osteoblastic Differentiation of Human Bone Marrow Stromal Cells on Hydroxyapatite/Bacterial Cellulose Nanocomposite Scaffolds.* Tissue Engineering Part A, 2009. **15**(5): p. 1091-1098.
80. Grande, C.J., et al., *Nanocomposites of bacterial cellulose/hydroxyapatite for biomedical applications.* Acta Biomaterialia, 2009. **5**(5): p. 1605-1615.
81. Chen, Y.M., et al., *In Vitro Cytotoxicity of Bacterial Cellulose Scaffolds Used for Tissue-engineered Bone.* Journal of Bioactive and Compatible Polymers, 2009. **24**: p. 137-145.
82. Evans, B.R., et al., *Palladium-bacterial cellulose membranes for fuel cells.* Biosensors & Bioelectronics, 2003. **18**(7): p. 917-923.
83. Zhao, Q., et al., *Surface Modification of Cellulose Fiber via Supramolecular Assembly of Biodegradable Polyesters by the Aid of Host-Guest Inclusion Complexation.* Biomacromolecules, 2010. **11**(5): p. 1364-1369.
84. Liebert, T., C. Hansch, and T. Heinze, *Click chemistry with polysaccharides.* Macromolecular Rapid Communications, 2006. **27**(3): p. 208-213.
85. Hasegawa, T., et al., *'Click chemistry' on polysaccharides: a convenient, general, and monitorable approach to develop (1 -> 3)-beta-D-glucans with various functional appendages.* Carbohydrate Research, 2006. **341**(1): p. 35-40.
86. Tingaut, P., R. Hauert, and T. Zimmermann, *Highly efficient and straightforward functionalization of cellulose films with thiol-ene click chemistry.* Journal of Materials Chemistry, 2011. **21**(40): p. 16066-16076.
87. Zhao, G.L., et al., *Heterogeneous "Organoclick" Derivatization of Polysaccharides: Photochemical Thiol-ene Click Modification of Solid Cellulose.* Macromolecular Rapid Communications, 2010. **31**(8): p. 740-744.

88. Andrade, F.K., et al., *Improving bacterial cellulose for blood vessel replacement: Functionalization with a chimeric protein containing a cellulose-binding module and an adhesion peptide.* Acta Biomaterialia, 2010. **6**(10): p. 4034-4041.
89. Lee, K.Y., et al., *Surface only modification of bacterial cellulose nanofibres with organic acids.* Cellulose, 2011. **18**(3): p. 595-605.
90. Bovey, F.A. and P.A. Mirau, *NMR of Polymers*. 1st ed. 1996, San Diego: Academic Press.
91. Pavia, D.L., et al., *A Small-Scale Approach to Organic Laboratory Techniques*. 3rd ed. 2011, Belmont, CA: Brooks/Cole Cengage Learning.
92. Qu, D., et al., *1,n-Alkanedithiol (n=2, 4, 6, 8, 10) Self-Assembled Monolayers on Au(111): Electrochemical and Theoretical Approach.* Bulletin of the Korean Chemical Society, 2009. **30**(11): p. 2549-2554.
93. Hamoudi, H., et al., *On the self assembly of short chain alkanedithiols.* Physical Chemistry Chemical Physics, 2008. **10**(45): p. 6836-6841.
94. Dong, S.J. and J.H. Li, *Self-assembled monolayers of thiols on gold electrodes for bioelectrochemistry and biosensors.* Bioelectrochemistry and Bioenergetics, 1997. **42**(1): p. 7-13.
95. Millone, M.A.D., et al., *Self-Assembly of Alkanedithiols on Au(111) from Solution: Effect of Chain Length and Self-Assembly Conditions.* Langmuir, 2009. **25**(22): p. 12945-12953.
96. Guo, Q., X. Sun, and R.E. Palmer, *Structural dynamics induced by self-assembled monolayers on Au(111).* Physical Review B, 2005. **71**(3): p. 5.
97. Lam, K.B., et al., *Bioelectrocatalytic self-assembled thylakoids for micro-power and sensing applications.* Sensors and Actuators B-Chemical, 2006. **117**(2): p. 480-487.
98. Seifert, M., M.T. Rinke, and H.J. Galla, *Characterization of Streptavidin Binding to Biotinylated, Binary Self-Assembled Thiol Monolayers-Influence of Component Ratio and Solvent.* Langmuir, 2010. **26**(9): p. 6386-6393.
99. Garton, A., *Infrared Spectroscopy of Polymer Blends, Composites and Surfaces*. 1st ed. 1992, Munich; New York; New York: Hanser Publishers ; Distributed in the U.S.A. and Canada by Oxford University Press.
100. Harris, D.C., *Quantitative Chemical Analysis*. 7th ed. 2007, New York, N.Y.: W. H. Freeman and Company.
101. Schramm, M. and S. Hestrin, *FACTORS AFFECTING PRODUCTION OF CELLULOSE AT THE AIR LIQUID INTERFACE OF A CULTURE OF ACETOBACTER-XYLINUM.* Journal of General Microbiology, 1954. **11**(1): p. 123-&.
102. Jones, G.O., D.H. Ess, and K.N. Houk, *Activation energies and reaction energetics for 1,3-dipolar cycloadditions of hydrazoic acid with C-C and C-N multiple bonds from high-accuracy and density functional quantum mechanical calculations.* Helvetica Chimica Acta, 2005. **88**(7): p. 1702-1710.
103. Binauld, S., et al., *Kinetic study of copper(I)-catalyzed click chemistry step-growth polymerization.* Journal of Polymer Science Part a-Polymer Chemistry, 2008. **46**(16): p. 5506-5517.

104. Zhou, B.J., et al., *Kinetic study of polysulfide-acrylate click reaction by DEA and DMA*. Polymers for Advanced Technologies, 2011. **22**(12): p. 2374-2381.
105. Lin, Y.-C., et al., *Synthesis, characterization and thermal properties of functionalized poly(2,6-dimethyl-1,4-phenylene oxide)s containing ethylenic, aldehydic, hydroxyl and acrylate pendant groups.* Polymer International, 2011: p. n/a-n/a.
106. Ifuku, S., et al., *Surface modification of bacterial cellulose nanofibers for property enhancement of optically transparent composites: Dependence on acetyl-group DS.* Biomacromolecules, 2007. **8**(6): p. 1973-1978.
107. Tong, X.M., et al., *A New End Group Structure of Poly(ethylene glycol) for Hydrolysis-Resistant Biomaterials.* Journal of Polymer Science Part a-Polymer Chemistry, 2011. **49**(6): p. 1513-1516.

APPENDIX

Appendix 1: ^{1}H-NMR stacked data for alkene peaks at 25^{0}C

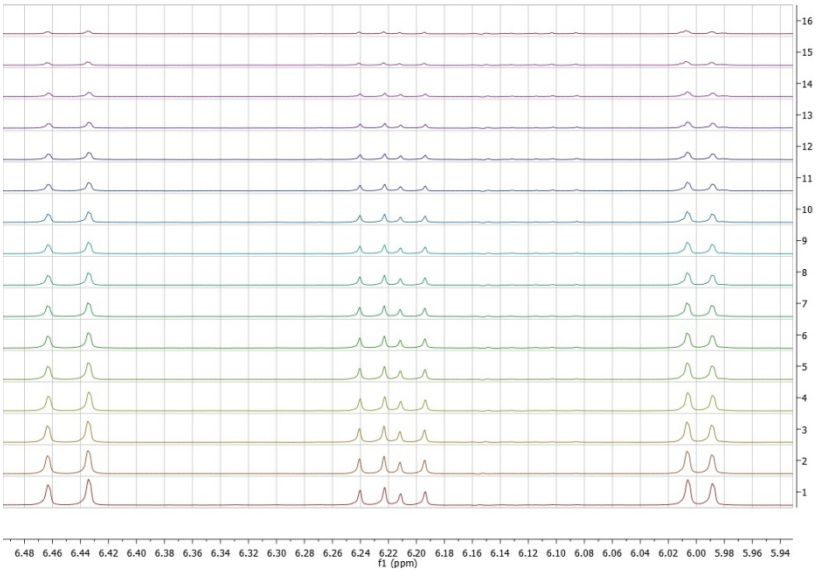

Appendix 2: ^{1}H-NMR stacked data for thiol and amine peaks at 25^{0}C

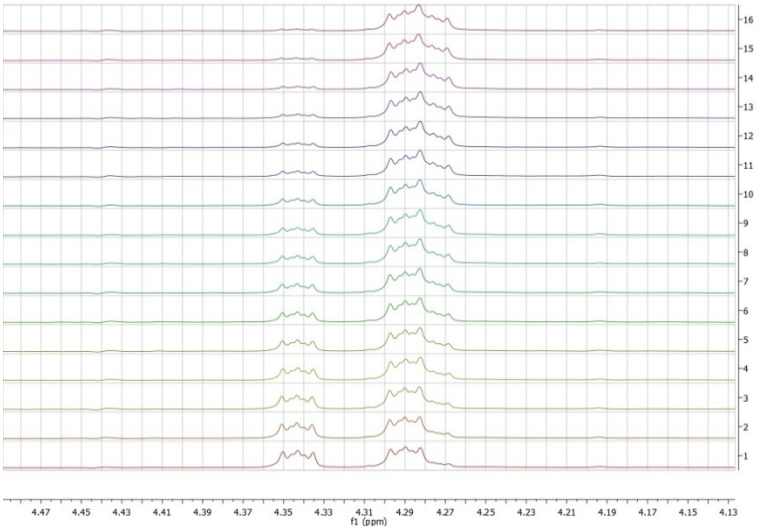

Appendix 3: ^{1}H-NMR stacked data for alkene peaks at 29^{0}C

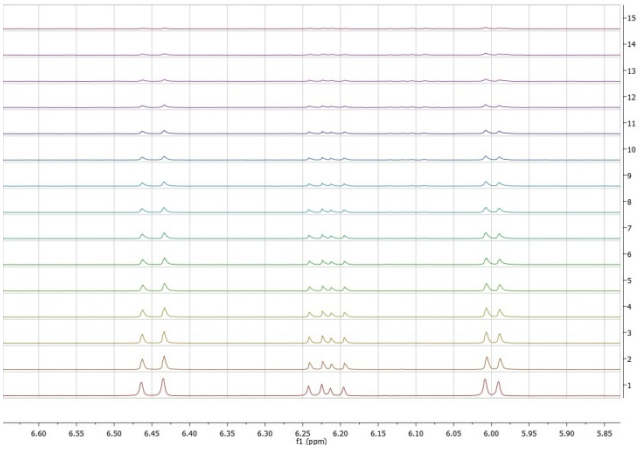

Appendix 4: ^{1}H-NMR stacked data for thiol peaks at 29^{0}C

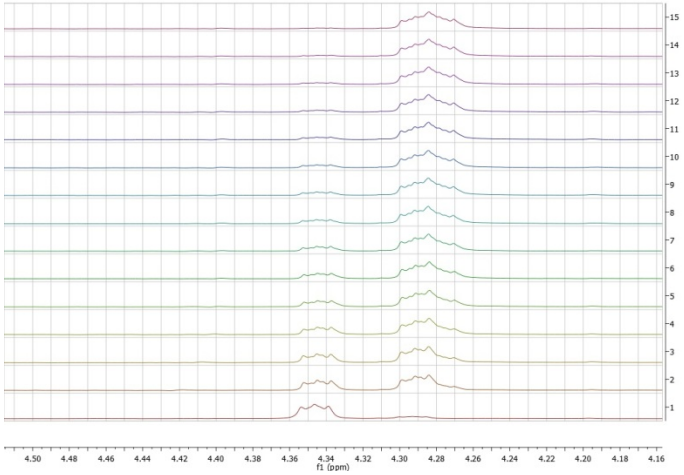

Appendix 5: ^{1}H-NMR stacked data for alkene peaks at 32^{0}C

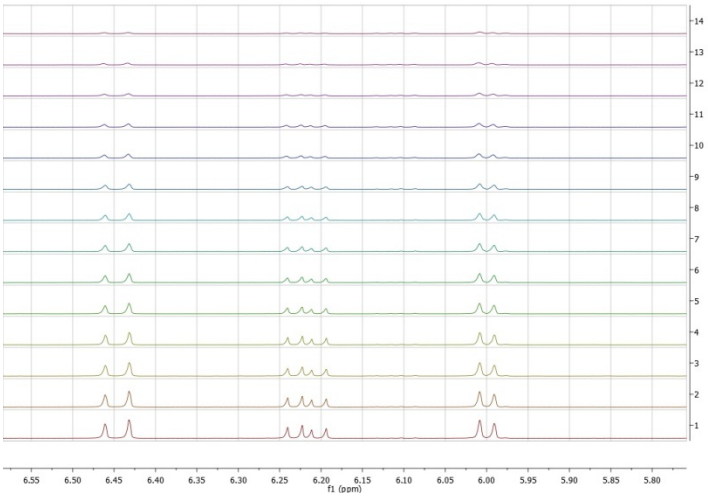

Appendix 6: ^{1}H-NMR stacked data for alkene peaks at 32^{0}C

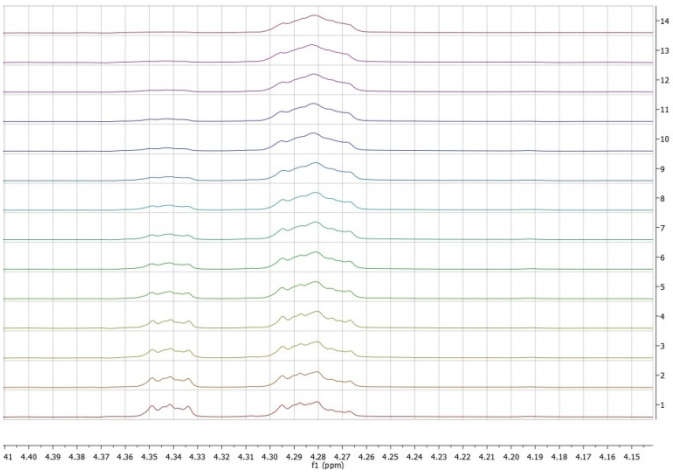

Appendix 7: MatLab ® program for determination of equivalence point for titration results.

```
% Kaan Serpersu
% Master's Thesis work
% Feb. 29th, 2012

% Objective: To determine the equivalence point from BC titration data,
% both native and modified BC by way of 1st derivative of
% titration data

clear all
clc

% Section for modified BC

% ph for modified BC as measured by ph meter
mph = [7.224 7.179 7.209 7.291 7.302 7.312 7.402 7.316  7.397 7.386 7.386
7.42 7.51 7.468 7.475 7.561 7.559 7.564 7.539 7.663 7.591 7.707 7.664 7.768
7.799 7.802 7.825 7.851 7.937 8.002 8.172 8.28 8.49 8.521 8.9 8.95 9.083
9.161 9.234 9.29 9.337 9.39 9.392];

% volume of titrant (NaOH) added to sample during titration
mvol = [36  37  38  40  42  44  46  48  50  52  54  60  62  64  66  68  70
72  74  78  82  86  90  94  98  102 106 112 118 124 130 136 142 148 154 160
166 172 178 184 190 196 202];

% Calculate average volume of titrant between each addition
% While loop will also calculate the change in pH and volume

a = length(mph);
b = 1;
y = 1;

while y < a
    avevol(b) = (mvol(b) + mvol(b+1))/2;
    cph(b) = abs(mph(b) - mph(b+1));
    cvol(b) = abs(mvol(b) - mvol(b+1));
    b = b + 1;
    y = y + 1;
end

% first derivative of the modified BC
fdmod = cph./cvol;

% equilavence point for modifed BC. Also display the volume and pH at this
% point

EPmod = max(fdmod(:));
[M,N] = find(fdmod == EPmod);
EPvol = mvol(N);
EPph = mph(N);

% Section for native BC

% ph for native BC as measured by ph meter

nph = [5.754 5.837 5.935 6.023 6.084 6.153 6.242 6.334 6.388 6.434 6.475
6.507 6.552 6.604 6.654 6.698 6.742 6.772 6.831 6.87 6.936 6.978 7.032 7.08
7.097 7.09 7.117 7.169 7.212 7.269 7.372 7.336 7.385 7.448 7.48 7.515 7.516
7.673 7.921 8.104 8.377 8.548 8.829 9.019 9.124 9.225 9.309 9.387 9.453 9.502
9.55 9.6 9.618 9.618 9.703 9.744 9.774 9.807 9.832 9.872];

% volume of titrant (NaOH) added to sample during titration
nvol = [1   2   3   4   5   6   7   8   9   10  11  12  13  14  15  16  17
18  19  20  21  22  23  24  25  26  27  28  29  30  31  32  33  34  35  36
37  38  40  42  48  54  60  66  72  78  84  90  96  102 108 114 120 126 132
138 144 150 156 162];

c = length(nph);
g = 1;
h = 1;

while h < c
    avevol(g) = (nvol(g) + nvol(g+1))/2;
    cph(g) = abs(nph(g) - nph(g+1));
    cvol(g) = abs(nvol(g) - nvol(g+1));
    g = g + 1;
    h = h + 1;
end

% first derivative of the modified BC
fdmod = cph./cvol;

% equilavence point for modifed BC. Also display the volume and pH at this
% point

EPmod = max(fdmod(:));
[Mn,Nn] = find(fdmod == EPmod);
EPvoln = nvol(Nn);
EPphn = nph(Nn);

% Print out findings to the front page

fprintf('The equivalence point for native BC is %4.3f pH and occured when
%2.0f microliters \nof titrant was added\n\n',EPphn, EPvoln)
fprintf('The equivalence point for modified BC is %4.3f pH and occured when
%3.0f microliters \nof titrant was added\n\n',EPph, EPvol)

% End of program
```

VITA

Kaan Serpersu was born on October 21st, 1984 in Baltimore, Maryland. His parents are Dr. Engin Serpersu and Faye Serpersu. Kaan received his high school degree in fall of 2002 from Bearden High School, went on to the University of Tennessee-Knoxville to earn a Bachelor's of Science degree in Biomedical Engineering with a minor in Materials Science and Engineering. Kaan has been extensively involved in the design and testing of a neural catheter with Oak Ridge National Laboratory, is continuing to work on a project with Y-12 in collaboration with Rusty Hallman and Dr. Benson, has three published papers with a fourth in submission, multiple poster presentations at both national and local conferences, and is aiming to pursue an engineering career in polymer and biomedical development.